Fall 12-15-2022

Noise And Propulsive Efficiency Interactions For Rotors And Propellers At Constant Thrust

Riccardo Roiati
Embry-Riddle Aeronautical University, roiatir@my.erau.edu

NOISE AND PROPULSIVE EFFICIENCY INTERACTIONS FOR ROTORS AND PROPELLERS AT CONSTANT THRUST

By

Riccardo Roiati

A Thesis Submitted to the Faculty of Embry-Riddle Aeronautical University

In Partial Fulfillment of the Requirements for the Degree of

Master of Science in Aerospace Engineering

December 2022

Embry-Riddle Aeronautical University

Daytona Beach, Florida

NOISE AND PROPULSIVE EFFICIENCY INTERACTIONS FOR

ROTORS AND PROPELLERS AT CONSTANT THRUST

By

Riccardo Roiati

This Thesis was prepared under the direction of the candidate's Thesis Committee Chair, Dr. Richard P. Anderson, Department of Aerospace Engineering, and has been approved by the members of the Thesis Committee. It was submitted to the Office of the Senior Vice President for Academic Affairs and Provost, and was accepted in the partial fulfillment of the requirements for the Degree of Master of Science in Aerospace Engineering.

THESIS COMMITTEE

Chair, Dr. Richard P. Anderson	Member, Dr. Kyle B. Collins
Member, Dr. Anastasios S. Lyrintzis	
Graduate Program Coordinator, Dr. Hever Y. Moncayo	Date
Dean of the College of Engineering, Dr. James W. Gregory	Date
Associate Provost of Academic Support, Dr. Christopher Grant	Date

To my dad, Fabio, my mom Cinzia, my grandmother Pierina and to the memory of my late grandfather, Francesco.

I wouldn’t be where I am today without your immense support.

ACKNOWLEDGEMENTS

I would like to take this opportunity to thank the following people, without whom I would not have been able to complete this research.

To my esteemed advisor and committee chair, Dr. Richard Anderson, for his invaluable knowledge, expertise, and patience in guiding me through this research as well as for awarding me the Graduate Research Assistantship position at the Eagle Flight Research Center. To Dr. Kyle Collins, co-chair of the committee, for his continuos support, encouragement and enthusiasm to assist and help in any way possible. To Dr. Tasos Lyrintzis for his expert counsel and support all throughtout my studies in the university, both at the undergraduate and graduate level.

I would like to express my gratitude to Xavier Santacruz for dedicating his time and knowledge to help me understand and master the research work he had previously done, so that I could build upon it and perform my own research without starting from ground zero.

I am extremely grateful to my family, for their immense support and sacrifices that have allowed me to live in the United States and pursue my dreams.

I would like to thank my loving wife, Malina, for her continuous support and selfless help.

I would like to thank the late Walter Wilson for taking me in as a 17 years old exchange student from Italy and mentoring and guiding me throughtout the years. Not only by making my goals his own but also by being my family while I was away from my home country.

I would also like to thank Rhett Carter, the Orcutt Academy High School Principal, in Orcutt, CA, for giving me the opportunity to earn my high school Diploma, which allowed me to continue my studies in the USA. I am beyond grateful for his continued support.

Lastly I want to thank my friends from the University and the Eagle Flight Research Center for creating a fun and enjoyable research experience.

ABSTRACT

In the emerging market of Advanced Air Mobility (AAM), aerospace companies have been designing and prototyping electric and hybrid vehicles to revolutionize travel. These vehicles must have low noise and particulate emissions while also having enough propulsive efficiency to complete the mission. This thesis aims to study the relationship between noise and propulsive efficiency as related to any aircraft equipped with an electric motor and a variable pitch rotor/propeller. The combination of the electric motor with the variable pitch propeller/rotor allows for a decoupled rotational speed and torque generation, meaning that the electric motor can generate the same amount of torque while operating at different rotational speeds. This feature allows the rotor/propeller to hold constant thrust at different combinations of rotational speeds and torque, by adjusting the collective pitch of the blades. This research will show that, for a rotor at constant thrust, the minimum noise (from loading and thickness contributions) and minimum power operating points in terms of rotor RPM and collective blade pitch, are not the same thus leading to the fact that it takes increased energy to decrease noise. A MATLAB code is developed to investigate the power and noise relationship by employing several functions to integrate XFOIL and Blade Element Momentum Theory for the rotor performance calculations and WOPWOP for thickness and loading noise analysis. Broadband noise is not included in the analysis herein. In addition, this thesis will present the design and build of a rotor test stand used to test rotors to validate the simulation results and provide hardware-based solutions for the power required by a rotor in hover. Based on the experimental and simulation results, a closed form equation is also proposed that shows the power required for a rotor at constant thrust, and it can be included in a preliminary rotor performance analysis for AAM vehicle design.

TABLE OF CONTENTS

LIST OF FIGURES

LIST OF TABLES

1 Introduction

The flying taxi has been the novel aviation concept of this era. The merging of technologies like Distributed Electric Propulsion (DEP) and digital Fly-By-Wire (FBW) flight control systems has allowed the development of numerous new electric vehicle designs and prototypes capable of vertical takeoff and landing. Advanced Air Mobility (AAM) companies aim to operate these aircraft in urban environments to offer a faster and more environmentally friendly way to commute.

Electric vertical takeoff and landing (eVTOL) technology offers a lot of flexibility in terms of vehicle design as a single DEP unit can easily be positioned on the vehicle's frame to create different geometries and ways to produce hover and forward thrust. For example, some vehicles are similar to a traditional helicopter, such as the Jaunt Air Mobility aircraft [1] shown in Figure 1.1 (A). Other vehicles incorporate several rotors or propellers like the Volocity [2] shown in Figure 1.1 (B). Other designs like the Aurora PAV [3] shown in Figure 1.2 (A) utilize a Lift plus Cruise configuration by having some DEP units to lift and other units to provide forward thrust. Other vehicles like the one designed by Joby Aviation [4] shown in Figure 1.2 (B), use tiltrotors to move from hover to forward flight.

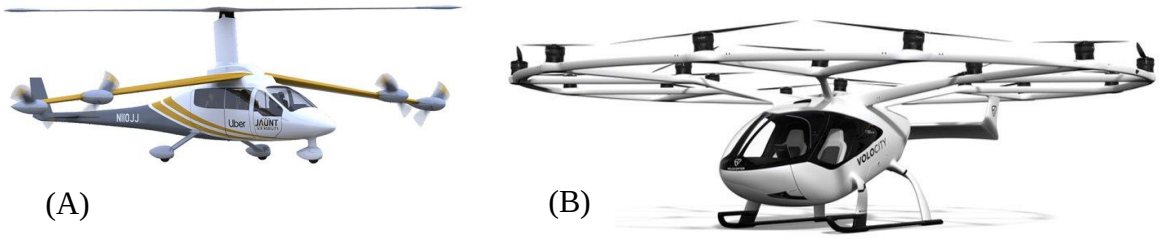

(A) (B)

Figure 1.1 Jaunt Air Mobility (A) [1], and the Volocity Aircraft (B) [2]

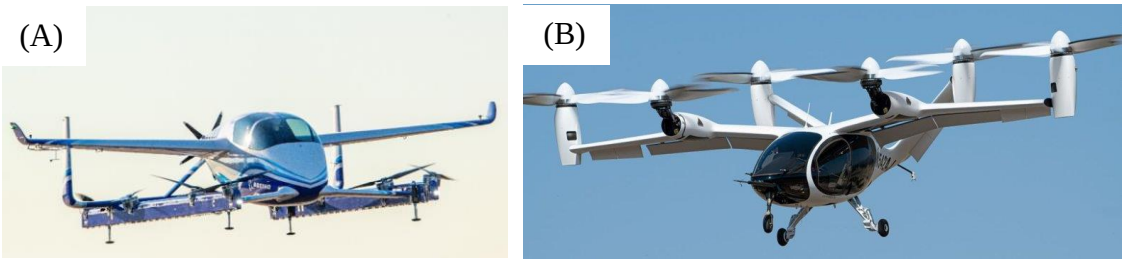

Figure 1.2 Aurora PAV (A) [3], and the Joby Aviation aircraft (B) [4]

Not only do AAM vehicles look different, but they also utilize different control methods to achieve changes in thrust and moment. Figure 1.3 below shows the 2 different control methods that are used. The simplest method to implement, shown in Figure 1.3 (A), is to use RPM control on fixed pitch propellers, which is a strategy identical to what is used on hobby-size drones. This simple strategy changes the thrust generated by the DEP unit by increasing or decreasing the RPM of the blades. A more advanced strategy, shown in Figure 1.3 (B), changes the thrust generated by the DEP unit by increasing or decreasing the RPM of the blades as well as their collective pitch angle.

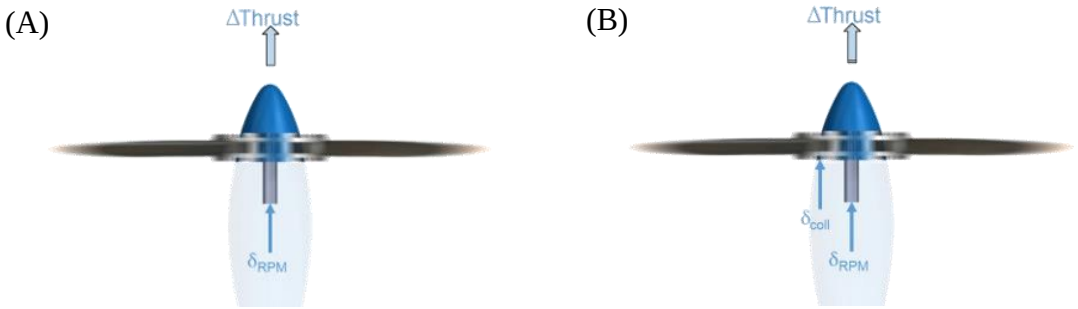

Figure 1.3 Thrust change by RPM only (A). Thrust change by collective pitch change and/or RPM change (B)

The main goals that the AAM industry has to meet for the successful implementation of its vehicles in an urban environment are: safety, low to zero emissions, low noise and high

efficiency. To have low to zero emissions, these vehicles are designed to be fully electric or hybrid. To prove their reliability and safety, many AAM companies are seeking FAA certification as mentioned by the acting FAA administrator Billy Nolen [5]. Low noise and high propulsive efficiency represent ongoing problems that must be solved. Having an efficient aircraft will result in a longer range which will increase the operational area around a city as well as the emergency reserves.

A survey from the European Union Aviation Safety Authority (EASA), based on responses from 3,690 citizens across six European cities, identified noise as one of the major concerns for societal acceptance of AAM [6]. Concerns about hearing loss largely focus on excessive noise exposure. But environmental noise is also a health hazard. People living in cities are regularly exposed to noise above 85 decibels from sources like traffic, subways, industrial activity, and airports [7]. That's enough to cause significant hearing loss over time. Urban life also sustains average background noise levels of 60 decibels, which is loud enough to raise one's blood pressure and heart rate, and cause stress, loss of concentration, and loss of sleep [7]. With the implementation of these AAM aircraft in cities, comes the need to have the right infrastructure to allow for their safe operation. Vertiports are the current viable concepts of city infrastructure that will be built to allow AAM vehicles to take off and land similarly to a helicopter landing pad on top of a building. The operation of AAM aircraft in vertiports will certainly increase the already high noise levels in cities and thus viable solutions should be found to minimize its negative impact and make these AAM aircraft quieter.

1.1 Literature Review

AAM noise reduction is a relatively new problem that needs to be solved, however helicopter noise has been investigated for many years and two different approaches can be taken to decrease it. The first approach is to utilize passive noise reduction techniques. The second

approach utilizes active noise reduction techniques, which are more complicated to implement. These approaches will be discussed in section 1.1.1.

One of the benefits of DEP comes from the use of electric motors. Electric motors operate differently than internal combustion engines, and their rotational speed is decoupled from torque generation. This feature can be a benefit in an attempt to decrease noise and improve propulsive efficiency and it will be presented in section 1.1.2.

1.1.1 Rotor Noise Reduction Techniques

Since AAM vehicles employ propellers or rotors, just like a helicopter, the first thing that can be done to decrease rotor noise is to focus on the blade geometry and design. Implementing blade geometry changes to lower noise is known as a passive noise reduction technique. A few techniques that have been proven to decrease noise will be presented below.

Employing a leading edge boundary layer tripping system made of aluminum adhesive tape has been shown to decrease tonal and total noise by forcing the flow to transition from laminar to turbulent [8]. This flow transition replaces the tonal noise, associated with laminar flow, with broadband noise radiating from the trailing edge of the blade [9]. A rendering is shown in Figure 1.4.

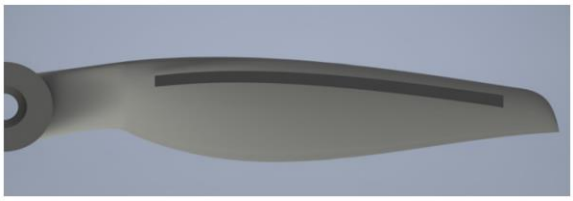

Figure 1.4 Boundary layer tripping system [9]

Owls are well known to fly really quietly [10]. Applying a serrated blade trailing edge to mimic an owl's wings has been shown to reduce noise generation in several studies to the expense of efficiency [11, 12, 13] from the destructive interference of the pressure fluctuations

produced by the flow structures along the slanted edges [9]. A rendering of a serrated blade is shown in Figure 1.5.

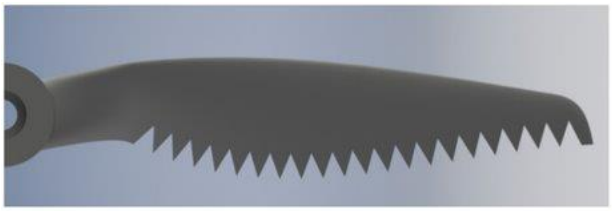

Figure 1.5 Serrated trailing edge [9]

Designing a bio-inspired blade with a planform shape that mimics a cicada wing has also been shown to decrease noise [14]. When compared to a baseline tapered blade, the bio-inspired blade could generate the same thrust at lower RPM thus emitting lower noise [14]. A rendering is shown in Figure 1.6.

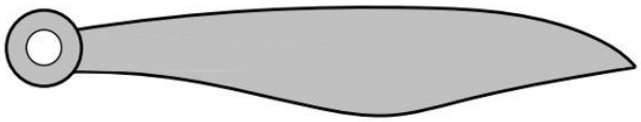

Figure 1.6 Bio-inspired blade [9]

A study from Joby Aviation tested several blades with different tip speeds and mean chord values for multiple collective pitch intervals [15]. By scaling up the mean chord of the baseline blade and reducing the operating RPM, the thrust generated by the propeller was kept constant for each collective pitch interval tested. They found that as the blade chord was increased and the tip speed decreased, the hover performance in terms of power loading decreased when compared to the baseline blade. In addition the torque required from the electric motor increased as tip speed decreased and the chord increased, thus requiring a larger and heavier motor. When looking at the noise reduction benefits however, decreasing the tip speed while also increasing

the mean blade chord to keep a constant thrust was found to lower the noise. The power loading and noise relationship is shown in Figure 1.7.

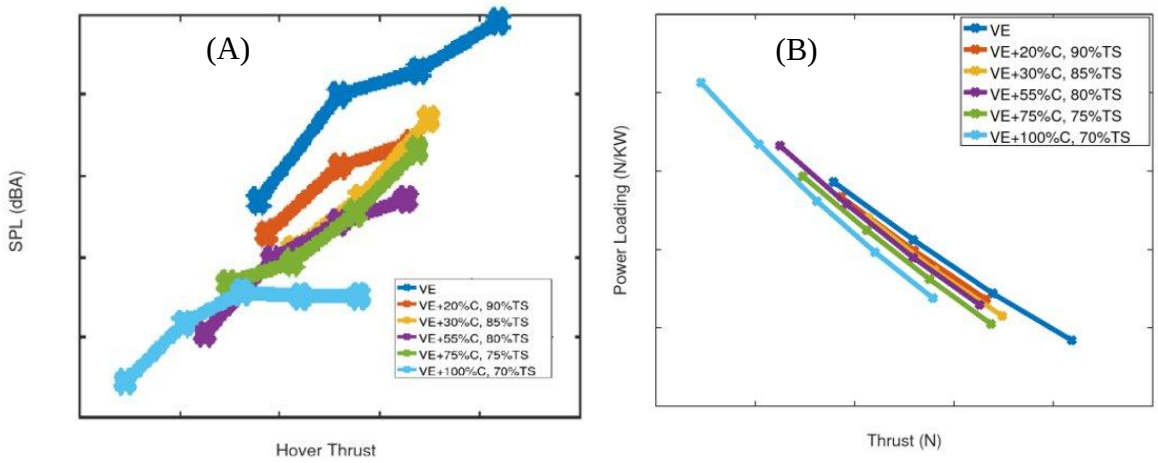

Figure 1.7 Hover Thrust vs. SPL (A). Hover Thrust vs. Power Loading (B). [15]

Joby Aviation concluded that a 55% chord increase and 80% tip speed decrease was ideal for their next blade design to minimize noise emissions.

In addition to optimizing the blade geometry to decrease noise, active techniques can be used to alter the operation of the blades during flight. This alteration can be done by a controller in an open loop or in a closed loop configuration where a parameter of choice such as blade surface pressure or noise measured by a microphone is used as a feedback variable to engage the control law.

Nihon University in Tokyo, Japan, [16] presented a way to decrease noise on a spinning rotor by engaging an active tab at the tip of the blade. Pressure transducers where installed on the blade to measure the blade surface pressure and then use it as the feedback variable for the control law. The tab, shown in Figure 1.8, was deflected back and forth during flight and was shown to decrease noise by 3 dB.

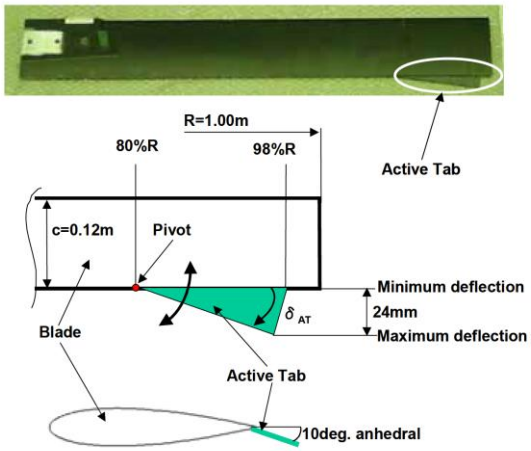

Figure 1.8 Active Tab Mechanism [16]

Individual blade root control, or individual blade control (IBC) is another active method utilized to decrease noise, specifically blade vortex interaction (BVI) noise, by controlling the blades individually and changing their pitch angle at different frequencies. This method has been shown to decrease noise by up to 5 dB when compared to a rotor spinning without any IBC input [17].

Higher Harmonic Control (HHC) can also be used to decrease noise. A study done by NASA Ames Research Center [18] carried out experiments on a XV-15 rotor equipped with actuators under the swashplate to provide HHC excitations. Blade pressure readings were used for the feedback controller, whose objective was to optimize the phase for HHC input of the 2/rev frequency to reduce the pressure signals. The study showed a 5.3 dB noise reduction when compared to the same rotor running without any HHC inputs. The test apparatus used is shown in Figure 1.9.

Figure 1.9 Rotor Test apparatus [18]

An interesting method to decrease noise was presented in the Journal of Aircraft by Padthe et al. in 2016 [19]. This method utilizes closed loop control to deflect microflaps on the blade. To simulate this approach, the authors used a CFD based aerodynamic model along with the code AVINOR to simulate the aerodynamic effects of the microflaps. WOPWOP was used for noise analysis. Figure 1.10 presents a rendering of the blade with microflaps.

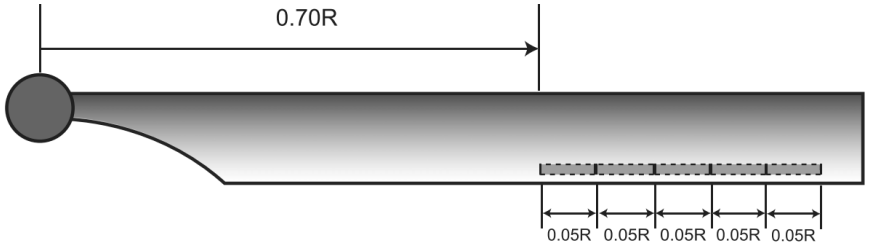

Figure 1.10 Microflaps Rendering [19]

An adaptive HHC algorithm for active noise reduction was used during a heavy BVI descending flight condition. This algorithm assumed that the helicopter can be represented by a

linear model relating the output to the control input and it employs feedback control from a microphone located on the helicopter. The control input used was a combination of 2/rev, 3/rev, 4/rev and 5/rev harmonic amplitudes of the control surface deflection. The researchers found that using 5 microflaps reduced noise by 6 dB. In addition, the study found that placing the microflaps closer to the blade tip was the most beneficial for noise reduction.

A potential noise reduction technique directly related to AAM is found in a patent application presented by Amazon [20] in 2018. This patent describes how to utilize noise phase cancellation to cancel out noise from drones by emitting anti-noises that have equal intensity and equal but out of phase frequencies. The physics behind this concept is that if two identical signals are 180° out of phase, they will completely cancel each other out. According to Amazon, 2 different control laws could be used to apply this principle successfully.

The first method would be to gather as much data as possible regarding the environmental conditions present in the most common routes that the Amazon drones fly to deliver packages to cities. After all the data is obtained, a machine learning process is used to calculate the sound that would be emitted at those environmental conditions. Therefore, during flight, the drone equipped with a controller would be able to recognize at which environmental conditions it is operating at and then speakers mounted on the frame of the drone will generate the anti-noise necessary to cancel out the noise. A diagram showing the environmental conditions going into the control law is presented in Figure 1.11. As the environmental conditions are always changing during the flight, the controller would be adapting the anti-noise generation accordingly.

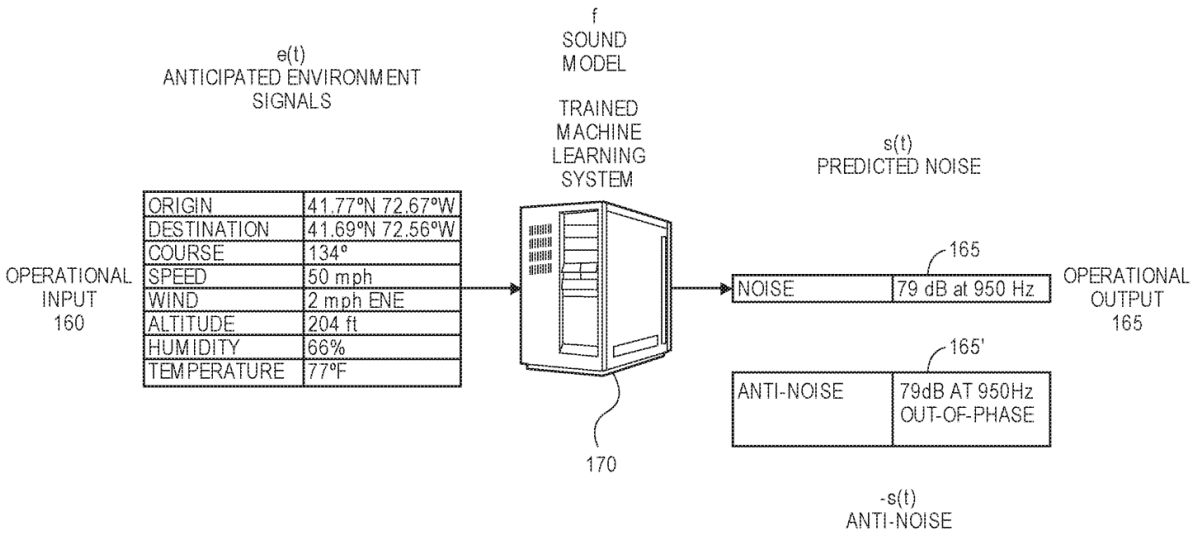

Figure 1.11 Noise Cancellation Method 1 [20]

The second method would be to have specific microphones on the drones able to measure noise directly and then generate the anti-noise necessary to eliminate the total noise. This method however will require more computation time and energy, and it would add weight to the structure, thus requiring more power to operate the drones.

Figure 1.12 below shows how anti-noise could be used, with a priority for urban and populated areas. In fact, as shown in the figure, no anti-noise is used when flying over water, or over a cemetery since those are not noise sensitive areas. This is done in order to save energy. When flying over moderate noise sensitive areas, only some anti-noise might be used, as shown when flying over a sporting venue, which is assumed to already be somewhat loud.

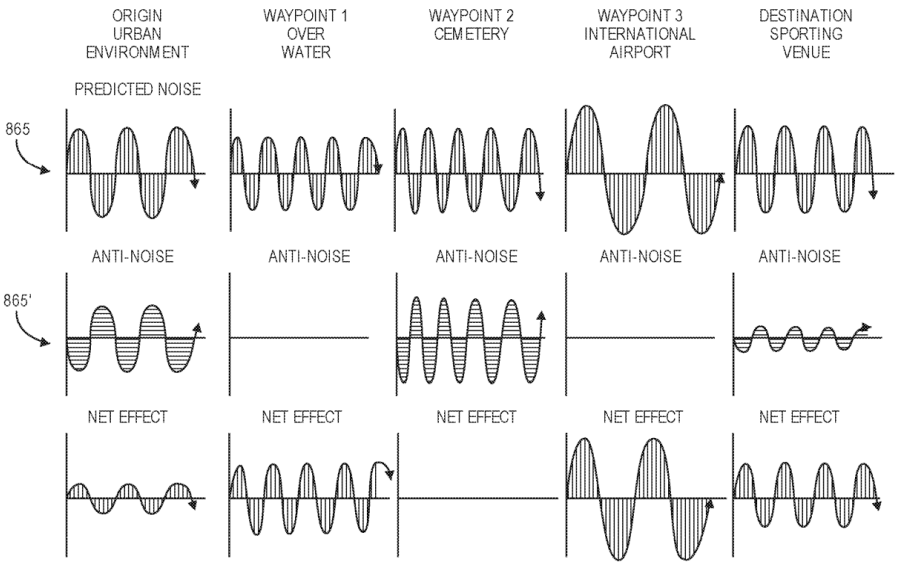

Figure 1.12 Application of the Anti-Noise principle [20]

1.1.2 Rotor Noise and Performance Prediction Techniques

When comparing noise generated from a helicopter to the one generated from an AAM vehicle, the very first distinction that can be made before looking at different blade designs, is the simple fact that the AAM vehicle uses one or more electric motors. When compared to a piston engine, the electric motor weighs less, has higher efficiency because of lower complexity and less moving parts and more importantly generates lower engine noise. In addition, a gasoline engine operates on a fixed torque versus RPM curve while any electric motor with an appropriate controller can vary torque and RPM independently [21]. This means that a gasoline engine has a single operating point for a required power output as shown in Figure 1.13, while an electric motor can have many torque and RPM combinations as shown in Figure 1.14 for the YASA750 electric motor [21].

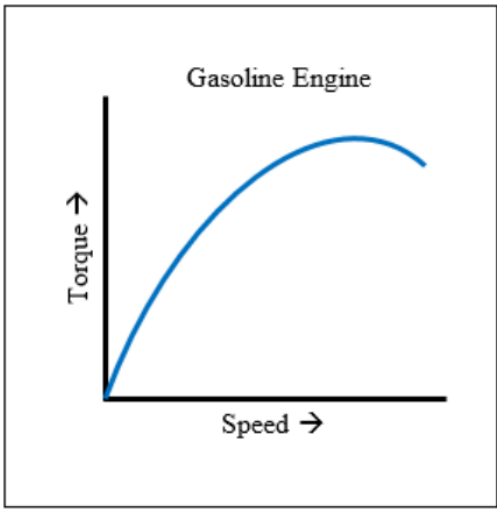

Figure 1.13 Gasoline engine torque vs. speed relationship [21]

The benefits of the electric motor combined with the use of a variable pitch prop-rotor are shown by Gartenberg's research work where he analyzes the performance and noise of a Diamond HK-36 propeller [21]. Gartenberg starts with the efficiency map of the YASA-750 electric motor operating at 700 volts shown in Figure 1.14. This efficiency map is given in terms of Torque and RPM. In the figure it can also be seen how the same torque can be generated at different RPM settings. He then digitizes an efficiency map for the controllable pitch MT-propeller as shown in Figure 1.15.

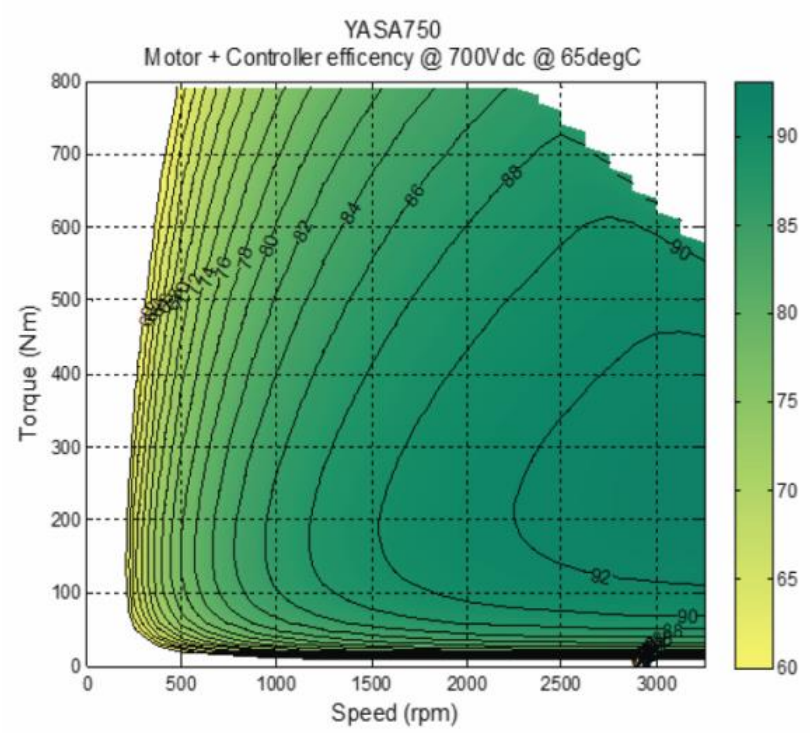

Figure 1.14 YASA-750 motor and controller efficiency map [21]

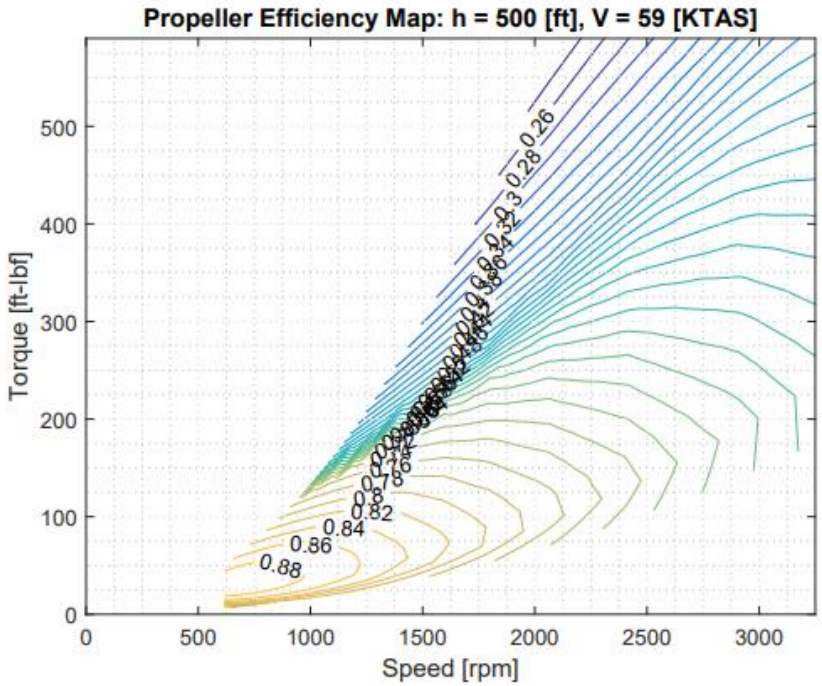

Figure 1.15 Propeller efficiency map [21]

The digitized motor efficiency map is then combined with the propeller efficiency map to generate a combined motor and propeller efficiency graph as shown in Figure 1.16. In the figure Gartenberg also shows a constant thrust curve of 500 lb. From the curve it can be seen how a constant thrust can be maintained at different operating RPM thanks to the variable pitch propeller.

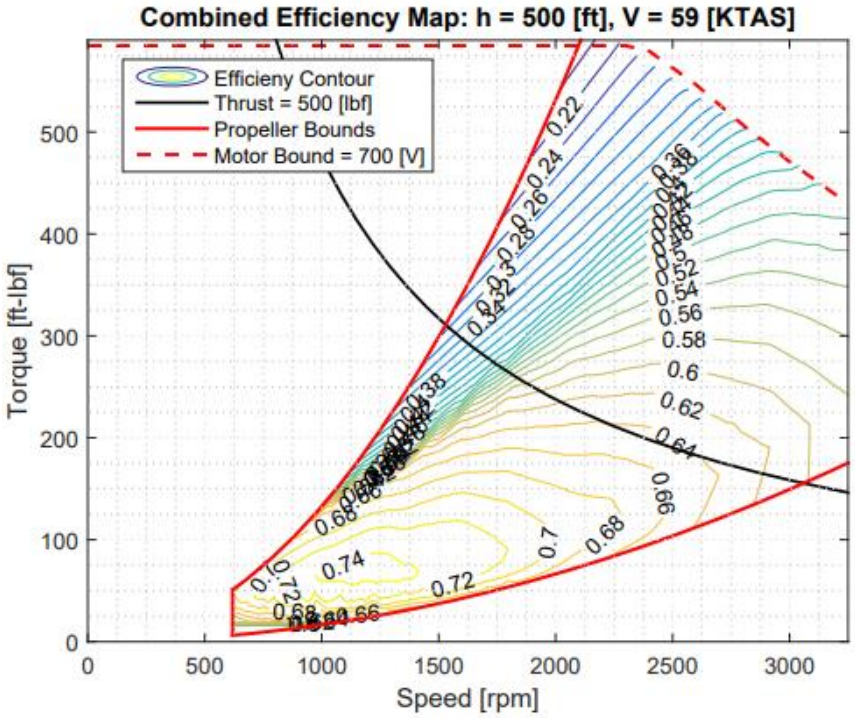

Figure 1.16 Motor and Propeller combined efficiency map with constant thrust curve [21]

Gartenberg uses the Hamilton Standard methodology to model the propeller noise at a given altitude and airspeed as shown in Figure 1.17.

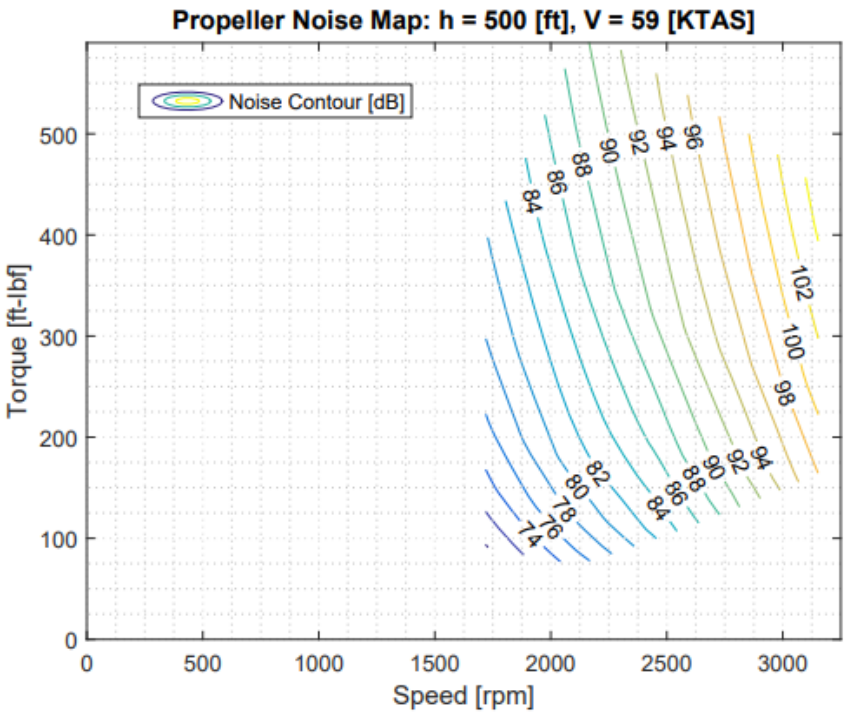

Figure 1.17 Propeller noise map with Hamilton Standard methodology [21]

Gartenberg then overlays the propeller noise map on the combined efficiency map for the motor and propeller. Figure 1.18 shows the combined efficiency map with the noise contour and a constant thrust line of 500 lb. By following the constant thrust curve in the figure, it is possible to see how efficiency and noise change and two different operating points become apparent. One that is at maximum efficiency but higher noise (indicated by the +) and one that is at lower noise but lower efficiency (indicated by the X).

Gartenberg shows that the ideal range is operating between the minimum noise and maximum efficiency, depending on what conditions must be met in the mission profile. The concept that vehicles with electric motors and variable pitch propellers can manipulate their operating conditions to alter their noise emission and power output was also awarded with a patent assigned to Embry Riddle Aeronautical University in 2021 [22].

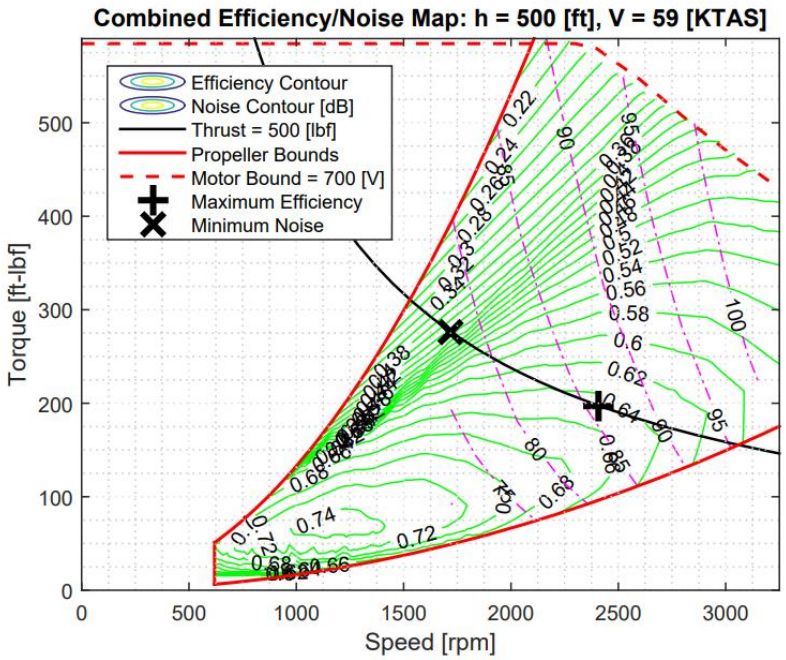

Figure 1.18 Location of maximum efficiency and minimum noise at constant thrust [21]

Following Gartenberg's work, Santacruz [23] developed an advanced tool to predict the performance and noise for a rotor or propeller in both hover and forward flight. The tool utilizes Blade Element Momentum Theory (BEMT) with MATLAB and Xfoil to evaluate the performance of a rotor/propeller and it also calculates the noise with PSU-WOPWOP. In his work Santacruz compares the noise levels of a rotor with rectangular blades to the noise levels of a rotor with blades designed specifically for low noise operations. Santacruz also successfully validates the code's predictive accuracy. For example, the performance analysis part of the code is validated with experimental tests found in the literature performed with a rectangular blade with a NACA 0012 airfoil. Figure 1.19 shows part of the validation, where the simulation results for the pressure coefficient around different blade radial positions are shown in red, and the experimental results are shown in blue.

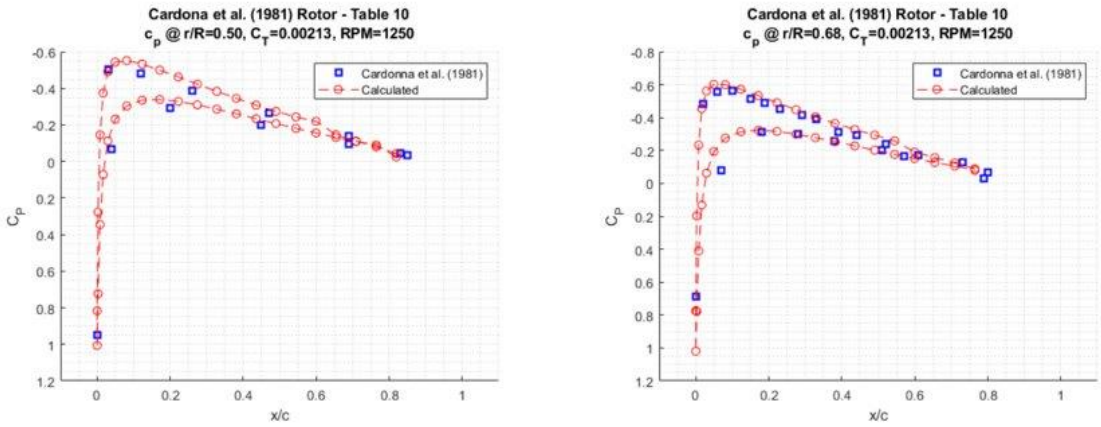

(a) $r = 0.50$ (b) $r = 0.68$

Figure 1.19 Tool's performance validation example [23]

Santacruz also successfully carries out the noise prediction validation, where he compares the noise calculated with his code to the noise presented in a WOPWOP test case for the 3-bladed Gyrodyne rotor. Figure 1.20 shows the acoustic pressure calculated with Santacruz's tool (in red) and the provided WOPWOP test case results (in blue). The results match very closely.

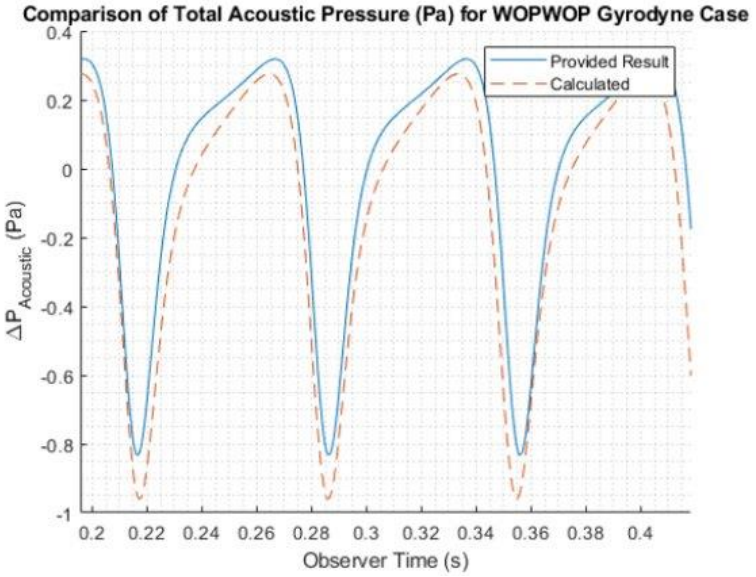

Figure 1.20 Tool's noise validation example [23]

1.2 Problem Statement

Following from Gartenberg's and Santacruz's work, the research presented focuses on the noise and power relationship applied to an AAM rotor in hover. This research aims to find an answer to whether it always takes more power to be quiet or if Gartenberg's finding was an isolated case that could only be applied to propellers in forward flight. The simple fact that it takes more power to be quiet could revolutionize the way that AAM vehicles are designed and operate. For example when landing or taking off from a vertiport in the city center, where noise is a big concern, the vehicle could operate in the low noise but low efficiency mode while it could operate at the high efficiency, high noise mode when noise is not a concern. Since AAM vehicles have limited energy reserves, and have limited range, minimizing the power required to operate at the low noise mode could be a new design goal from manufacturers to ensure a quiet aircraft in the most noise sensitive part of the mission profile: in the city center. The current thesis investigates the possibility of having a propeller or rotor designed to have the same maximum efficiency and minimum noise operating points while holding constant thrust. In addition a method is developed to predict the relationship between noise and power required to hover.

1.3 Objectives

The primary objective of this thesis work is to provide an accurate relationship between noise and power required to hover in order to investigate if a rotor or propeller takes more power to decrease noise emissions at constant thrust. Additional research objectives are listed below:

1) Develop a custom Blade Element Momentum Theory (BEMT) code and integrate it with the MATLAB functions previously developed by Santacruz [23] in order to analyze custom blade geometries.
2) Design and build a test stand to test different rotor blades. Equip test stand with a 6 degrees of freedom (6-DOF) load cell and a reliable data acquisition system to read forces and moments produced by the rotor. Use this data for further algorithm validation.
3) Use simulation and experimental results to investigate the noise and power relationship at constant thrust. This thesis focuses only on the loading and thickness noise contributions, while broadband noise will be subject of future work, as it could play an important role especially at high collective pitch deflections.
4) Develop a closed-form expression to calculate rotor power required in hover at constant thrust to be included in the design cycle analysis of an AAM vehicle.

1.4 Presented Work Outline

The research performed has been divided into two main sections:

1) **Methodology:** this section has been subsequently divided into 4 subsections:
    - Subsection 1: presents the BEMT theory, equations and assumptions used for the performance analysis of a rotor at constant thrust.
    - Subsection 2: presents the aeroacoustics theory, equations and assumptions used for noise analysis of a rotor at constant thrust. This subsection also presents an overview of how the MATLAB code has been created with reference to Santacruz's [23] previous work.
    - Subsection 3: presents the design and build of a Rotor Test Stand (RTS) as well as the cutting-edge equipment and techniques used for testing, data analysis and data post-processing.
    - Subsection 4: presents the derivation of a closed form equation for the hover power required of a rotor at constant thrust as a function of RPM.

2) **Results & Discussion:** this section presents and compares the results obtained from the 3 different methods presented in the methodology section. Experimental results obtained from testing with the RTS will first be used to validate the simulation results and then results from different constant thrust cases will be presented and compared between the RTS, simulation and the closed form equation. Important conclusions will be drawn and limitations will be discussed.

2 Methodology

Three different methods are used to find the answer to whether it takes more energy to decrease noise for a constant thrust condition. Figure 2.1 shows a flowchart that represents the methodology used in this research. First a simulation is used to calculate the performance and noise of a defined rotor of choice. Experimental tests are used to provide results for the rotor performance as well as to validate the simulation. The last step of the methodology entails proposing a closed-form expression that quickly provides a solution for the power required at a constant hover thrust condition.

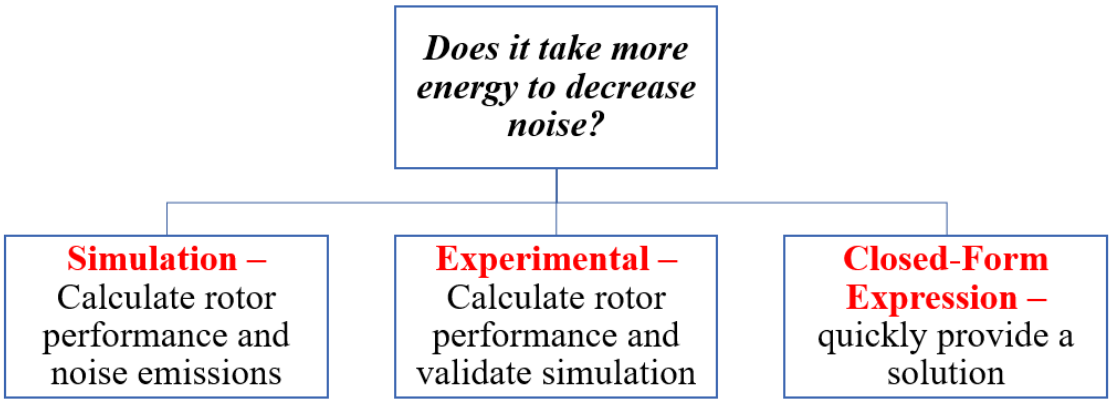

Figure 2.1 Methodology flowchart

The three different approaches will be discussed in the following sections. Section 2.1 and section 2.2 will discuss the theory that is used in the simulation. Section 2.3 will describe the design and build of a rotor test stand used for experimental tests, and section 2.4 will cover the proposed closed-form equation.

2.1 Blade Element Momentum Theory

Blade Element Momentum Theory (BEMT) as explained by Leishman [24] can be used to estimate the inflow distribution along the blade, and that inflow can be used to calculate the

thrust and power of a single blade. Any helicopter textbook contains complete derivations of the BEMT and this section will focus on the application of its most important equations that were used to create a MATLAB tool capable of calculating the thrust and power of a rotor in hover. Santacruz [23] previously developed a MATLAB code that implements BEMT with Xfoil to estimate the inflow and the aerodynamic coefficients (Cl and Cd) needed to calculate the thrust and power of a blade. In this work a custom BEMT code with blade tip losses is developed and integrated with the MATLAB functions previously developed by Santacruz [23] that employ Xfoil and WOPWOP for performance and noise analysis. The explanation of the concept behind the BEMT is presented below for a hover condition.

Considering the rectangular untwisted and untapered blade as shown in Figure 2.2, and focusing on a small element of the blade, the elemental thrust coefficient produced by the small blade element can be calculated from:

$$dC_T = \frac{1}{2}\sigma C_l r^2 dr \tag{2.1}$$

Where σ is the rotor Solidity:

$$\sigma = \frac{N_b c R}{A}$$

- N_b is the number of blades.
- c is the blade chord.
- R is the blade radius.
- A is the rotor disk area.
- C_l is the lift coefficient of the elemental blade section.
- r is the non-dimensional radial position.

- dr is the non-dimensional length of the elemental blade section at the radial position r.

By adding all the elemental thrust coefficients along the whole length of the blade, the total thrust coefficient can be calculated.

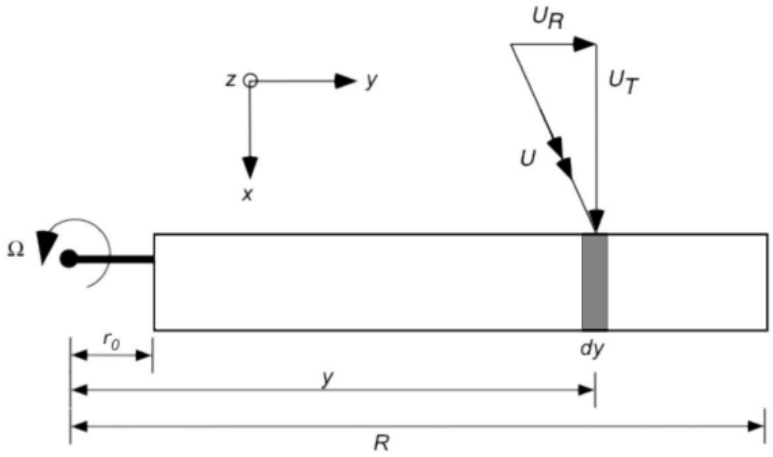

Figure 2.2 Top view of the blade showing a blade element in gray [24]

Similarly to the elemental thrust coefficient, an elemental power coefficient can be calculated with the BEMT and is divided into the induced power coefficient and the profile power coefficient. Their respective elemental values at each section of the blade can be calculated and then integrated for the whole blade to find the total power required with the following formula from Leishman [24]:

$$C_P = C_{Pi} + C_{P0} = \int_{r=0}^{r=1} dC_{Pi} + \int_{r=0}^{r=1} dC_{P0} = \int_{r=0}^{r=1} \lambda dC_T + \int_{r=0}^{r=1} \frac{\sigma}{2} C_d \, r^3 dr \qquad (2.2)$$

Where:

- λ is the inflow.
- C_d is the drag coefficient of the elemental blade section.

By looking at equation 2.1 and 2.2, the need to estimate the inflow as well as the C_l and C_d values becomes apparent. By applying Prandtl's tip loss function as shown in Leishman [24], the inflow can be found by iteration with the following equations:

$$\lambda = \frac{\sigma C_{l\alpha}}{16F}\left(\sqrt{1 + \frac{32F}{\sigma C_{l\alpha}}\theta r} - 1\right) \tag{2.3}$$

Where:

- $C_{l\alpha}$ is the airfoil lift curve slope.
- θ is the total pitch angle of the blade section.
- F is Prandtl's tip loss factor:

$$F = \left(\frac{2}{\pi}\right)\cos^{-1}(\exp(-f))$$

Where:

$$f = \frac{N_b}{2}\left(\frac{1-r}{r\phi}\right)$$

- ϕ is the induced inflow angle.

$C_{l\alpha}$ must be calculated first in order to carry out the iterations. For this reason Xfoil, written by Drela [25], can be used by assuming that the lift curve slope will stay constant for all future calculations.

Xfoil uses a high-order panel method and a fully coupled viscous/inviscid interaction method to evaluate drag, boundary layer transition, and separation [26]. With Xfoil Cl and Cd can be calculated for every elemental section of the blade. The inputs needed by Xfoil are the local Reynolds number and Mach number as well as the angle of attack of the elemental blade section. For a pre-determined blade geometry, collective pitch and RPM, these values can be readily calculated and fed to Xfoil to return the coefficients of interest.

The step by step approach used to apply the BEMT and Xfoil in MATLAB is described below following the user's input for the blade planform, RPM and collective pitch.

1) Xfoil is run for a range of angles of attack to calculate the average lift curve slope. The Reynolds and Mach numbers are calculated along the blade from the planform geometry and RPM input from the user.
2) Prandtl's tip loss function is iterated along with the inflow until a solution is reached. The elemental induced inflow angle along the blade can now be calculated.
3) The induced inflow angle is used to calculate the effective elemental angle of attack of all the blade sections and the inflow is used to calculate the resultant velocity at the blade element which is then used to calculate the local blade section Reynolds number and Mach number.
4) Xfoil is run again with the updated Mach number, Reynolds number and angle of attack of the blade sections. Xfoil calculates the lift, drag and power coefficients for each blade element.
5) Equation 2.1 and 2.2 are integrated across the whole blade to calculate the thrust and power for the rotor.

2.2 Aeroacoustics Theory

Figure 2.3 shows that rotor noise can be divided into harmonic noise due to its periodic and discrete frequency spectrum, and broadband noise due to its continuous behavior in the frequency domain [27]. The harmonic noise is then divided into loading and thickness noise. Loading noise can be attributed to the aerodynamic loading and unsteady forces on the surface of the blades and thickness noise can be attributed to the displacement of the air due to the thickness of the rotating blades. Some factors that cause broadband noise are turbulent incoming flow [27, 28], turbulent boundary layer interactions with the trailing edge of the airfoil [28, 29] and separation around the blade [27, 28].

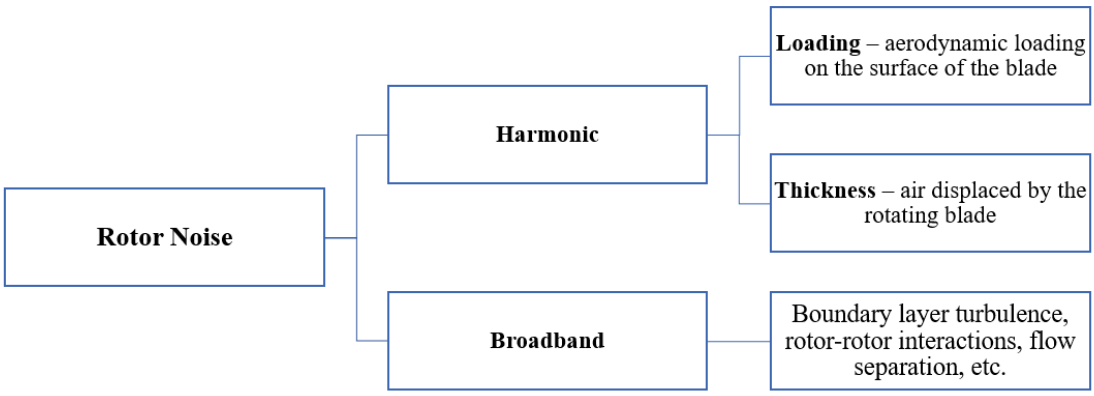

Figure 2.3 Rotor noise sources

Loading and thickness noise contributions can be predicted with Brentner's PSU-WOPWOP [30] that employs the Farassat Formulation 1A of the Ffowcs Williams-Hawkins (FW-H) equation. This equation is written in terms of the acoustic pressure due to thickness and loading and it calculates the total pressure fluctuation over the blade surface at the retarded time, namely the time when the sound is emitted, as shown by Lyrintzis [31], Farassat [32], and Brentner [33].

The thickness pressure contribution is given by:

$$4\pi P_T'(x,t) = \int_{f=0}\left[\rho_0 \frac{\dot{v_n}}{r(1-M_r)^2} + \frac{\rho_0 v_n \hat{r_i}\dot{M_i}}{r(1-M_r)^3}\right]_{ret} dS + \int_{f=0}\left[\frac{\rho_0 c v_n (M_r - M^2)}{r^2(1-M_r)^3}\right]_{ret} dS \quad (2.4)$$

The loading pressure contribution is given by:

$$4\pi P_L'(x,t) = \frac{1}{c}\int_{f=0}\left[\frac{\dot{l_r}}{r(1-M_r)^2}\right]_{ret} dS + \int_{f=0}\left[\frac{l_r - l_M}{r^2(1-M_r)^2}\right]_{ret} dS + \frac{1}{c}\int_{f=0}\left[\frac{l_r\left(r\dot{M}_r + c(M_r - M^2)\right)}{r^2(1-M_r)^3}\right]_{ret} dS \quad (2.5)$$

The total acoustic pressure is found by adding the 2 pressure contributions written above, where:

- v and M are the velocity and Mach number terms that have to do with the blade motion.
- M_r is the Mach number in the radiation direction.
- $\dot{M}_r$ is the rate of change of the Mach number in the radiation direction with respect to the source time.
- $\hat{r_i}$ is the component of the unit radiation vector.
- l terms indicate the loading on the blade determined by the blade pressure distribution.
- ρ_0 is the density of the undisturbed medium.
- r is the distance between the observer and the source.
- v_n is the local normal velocity of the blade surface.
- $\dot{v_n}$ is the rate of change of the normal velocity with respect to the source time and is deemed by Brentner to have a very small effect [33].

- c is the speed of sound in the undisturbed medium.
- f represents the moving surface (f = 0 for a fixed observer position).
- dS is the elemental blade surface area.

Santacruz [23] wrote the MATLAB function used in this research to call WOPWOP to calculate the noise and validated its output successfully. All that is needed to run WOPWOP is the pressure distribution along the blade of interest (calculated with Xfoil) and an observer position from where to run the analysis.

Greenwood et al. [34] presented results for a notional eVTOL rotor at constant thrust that show a very interesting trend. Farassat Formulation 1A was used to calculate the thickness and loading noise, while the Brooks, Pope, and Marcolini (BPM) method was used to estimate the broadband noise. Figure 2.4 shows the different noise contributions as well as the total noise. It is implied in the graph that while the tip Mach number decreases, the collective pitch of the rotor blades increases to maintain a constant thrust of 562 pounds.

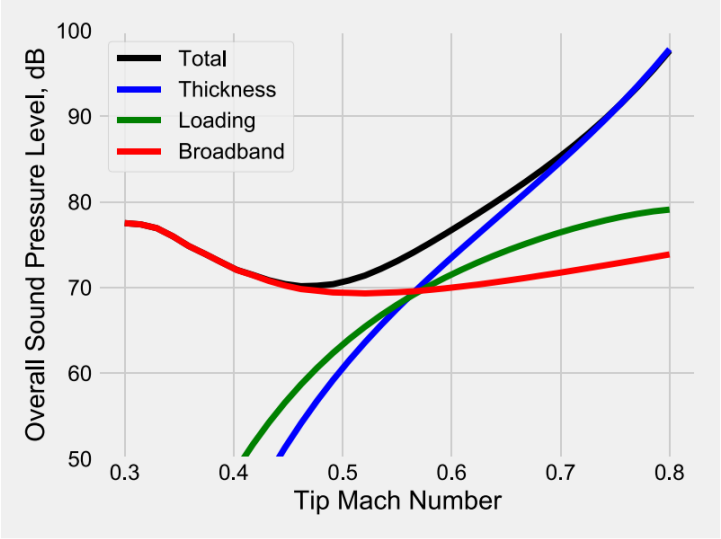

Figure 2.4 Variation of noise by tip Mach number for notional eVTOL rotor at constant thrust [34]

By looking at Figure 2.4, it can be concluded that both thickness noise (shown in blue) and loading noise (shown in green) decrease with decreasing RPM or tip Mach number. Tip speed in fact is the major factor that affects rotor noise from thickness and loading contributions, and decreasing the RPM will decrease noise as also shown by Farassat [35]. When looking at broadband noise (shown in red) however, it can be noticed how there is a point in which continuing to decrease the tip Mach number actually starts increasing the broadband noise, which leads to an increase of the total noise, shown in black. It can be noted that at high tip Mach numbers, thickness noise becomes the dominant source, while broadband noise becomes dominant at low tip Mach numbers. Broadband noise could in fact become prominent when the blades are operated at such a high collective pitch deflection that stall is reached and the flow around the blade separates. Therefore, for the case of a single rotor, the minimum noise point is found by decreasing RPM and reaching the point where broadband noise is at its minimum, possibly before separation or blade stall occurs. Broadband noise prediction is currently an area of active research, and the research work presented herein is focused only on the loading and thickness noise contributions.

Figure 2.5 below shows how the rotor performance and noise analysis is carried out in the MATLAB code:

- The user inputs the rotor parameters (RPM, Collective and blade geometry) and the observer position for noise analysis. Analysis switches can be used to turn off the noise analysis and only run Xfoil and BEMT for performance calculations.
- The BEMT calculates the Inflow, angle of attack and speed and Xfoil is used to return the aerodynamic coefficients for each blade section.
- BEMT calculates the thrust, power and torque for the user defined rotor.

- WOPWOP uses the pressure distribution calculated with Xfoil to calculate noise with Farassat's 1A Formulation.

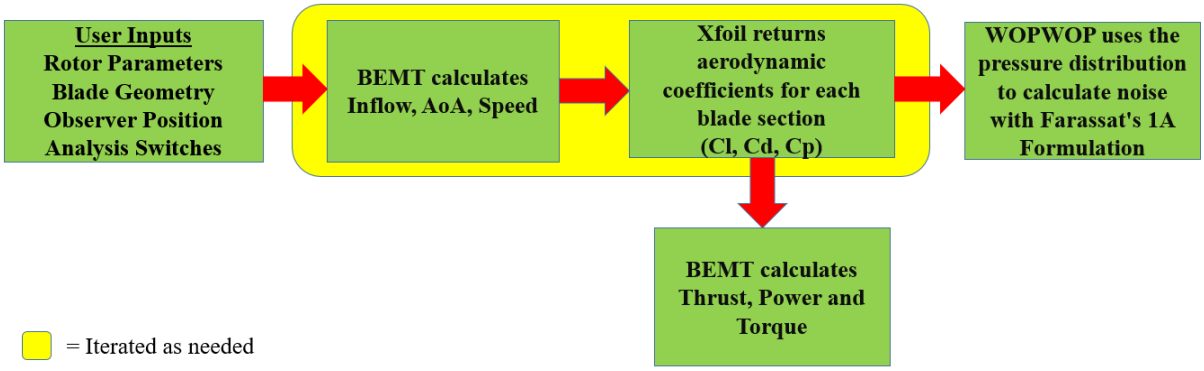

Figure 2.5 MATLAB Code Flowchart (Xfoil, BEMT & WOPWOP Integration)

2.3 Rotor Test Stand Design & Build

Fabrication of the Rotor Test Stand (RTS) structure was completed in August 2021. The RTS was developed by the author at the Eagle Flight Research Center (EFRC) for a Federal Aviation Administration (FAA) sponsored research project and it served different uses. For this reason numerous iterations have been made on the test stand's hardware and software, including the DEP unit design as well as its telemetry and data acquisition capabilities.

Figure 2.6 shows a CATIA-rendered structural model of the RTS. The structure consists of:

1. Three 1/4" thick A36 Steel Plates (12"x12", 10"x10", 8"x8") for mounting the hardware.
2. One 5 ft. Long A500 square steel tube (4x4x1/4 wall).
3. Two 4 ft. long A500 square steel tubes (4x4x1/4 wall) at the base.
4. Three 3'4" A500 square steel tubes (4x4x1/4 wall) at the base.
5. Four 3'6.5" A500 square steel tubes (4x4x1/4 wall) for lateral supports.
6. 4 swivel casters with wraparound break (400 lb. capacity each) for mobility.

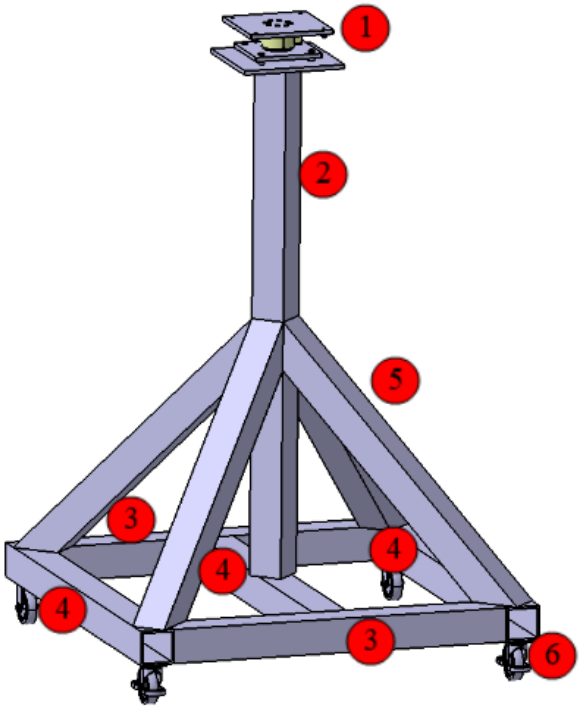

Figure 2.6 Rotor Test Stand CATIA Design

Developing a DEP unit to mount on the RTS was the first major challenge to overcome. The RTS offered the capability to test different DEP unit structures, referred to as "pods," mounted on the steel plate at the top of the stand. Figure 2.7 shows the first DEP pod design mounted on the RTS by the author and the EFRC research team to start running some preliminary tests. The first pod was put together from an off-the-shelf RC helicopter frame. As a matter of procedure, for all tests the RTS is tethered to the ground and enclosed by a large safety cage to arrest debris in the event of a catastrophic failure.

Figure 2.7 First DEP Pod Design

Several tests were run with this first design until the lateral supports started to bend due to the high vibrations during flight as shown in Figure 2.8.

Figure 2.8 DEP pod design 1 supports buckle due to high vibrations

The first DEP pod design's shortcomings gave the author and the EFRC team an opportunity to improve on future designs. The second design was conceptualized and implemented shortly after the failure of the first design. Its structure was composed of 3003 aluminum side plates bolted to 3-D printed PLA end caps, with the rotor tray mounted on top with screws and a 4" aluminum square tube mounted to the bottom. The second DEP pod was made much shorter than the first design to reduce vibrations. The inside of the pod housed the transmission belt and gearing between the rotor and motor shafts. Figure 2.9 shows the progression from a cardboard model to a complete assembly.

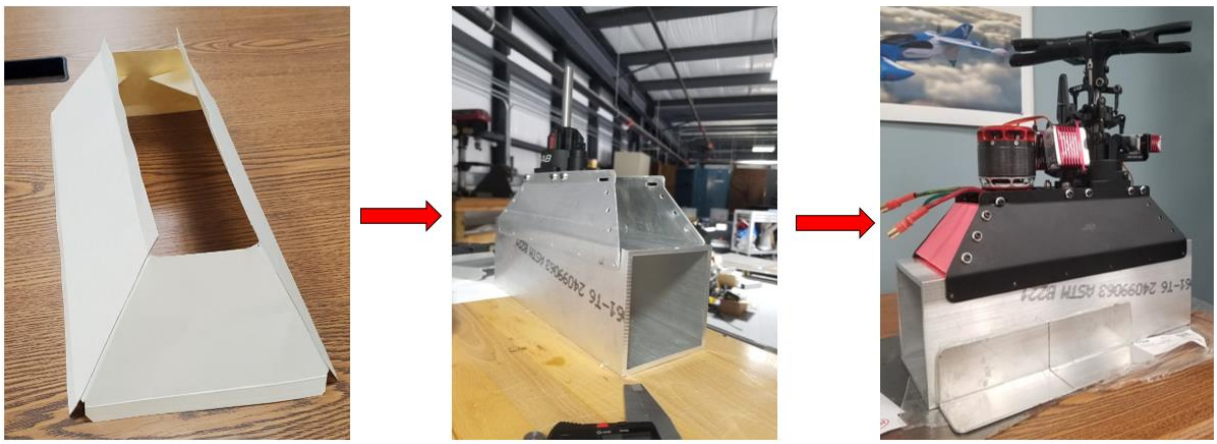

Figure 2.9 Second DEP Pod Design Flow

The final RTS design is shown in Figure 2.10. The DEP pod system consists of:

- Helicopter rotor mechanics from a SAB Goblin Raw 700 RC helicopter integrated with the EFRC distributed electric propulsion pod.
- Symmetric rectangular blades with a NACA 0015 airfoil called the “Goblin” blades.
- Kontronik Pyro 750-50 brushless outrunner electric motor.
- Kontronik Kosmik 200A speed controller.

- Two 6S 5000 mAh LiPo batteries connected in series for 50 V total.

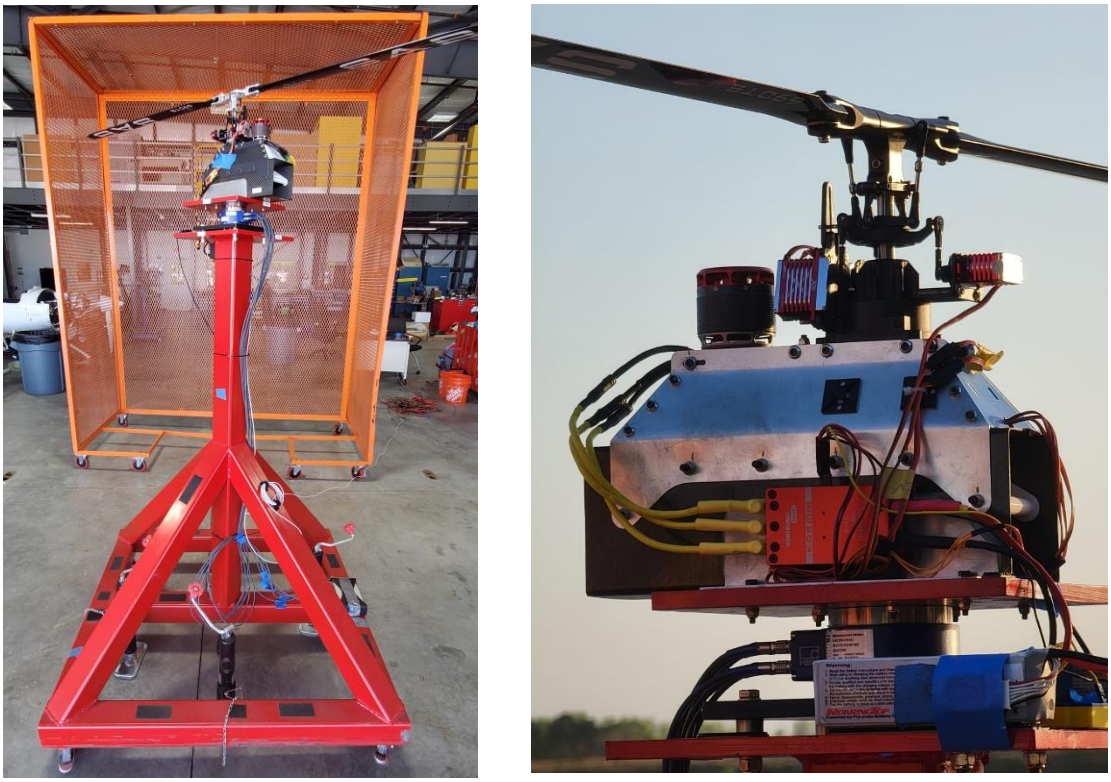

Figure 2.10 Rotor Test Stand Final Configuration

The RTS Data Acquisition System is made up of different components:

- A 6 Degrees of Freedom (6-DOF) Load Cell manufactured by HBM that allows for forces and moments measurements in all 3 axes (X,Y,Z). The Load Cell can measure a vertical force up to 2400 lb. and is shown in Figure 2.11 (A).

- A Quantum X MX840B data acquisition unit manufactured by HBM that allows for data sampling up to 48 kHz shown in Figure 2.11 (B). The Quantum X easily connects to the Load Cell to allow for a quick setup process and is capable of reading up to 8 different channels.

- The “Catman” software used to interface with the Quantum X to acquire and visualize the data live coming from the Load Cell. The software environment is shown in Figure 2.11 (E). The data is saved as a .MAT MATLAB file after every test.
- An ACT-3X Panel Tachometer from Monarch Instrument with a Remote optical LED sensor used to read the RPM of the rotor is shown in Figure 2.11 (C). The sensor emits a red LED light that is then reflected on the reflective tape under the rotating blades. The readings from the sensor are processed and displayed by the tachometer in real time. A second computer is used to communicate with the tachometer in real time through the Monarch Instrument custom software, PmRemote. This software allows the user to display the live RPM values on the computer screen while also saving the readings in an Excel file for post-processing.
- A speed controller shown in Figure 2.11 (D) is used to control the rotor and to log voltage and current to a micro SD card. This allows a calculation of the system’s operating power.

Figure 2.11 Load Cell (A). Quantum X (B). Tachometer setup (C). Speed Controller (D). Catman software environment (E).

To accurately control the commanded RPM and deflections, MATLAB/Simulink was used to create a code that integrates with an Arduino Mega board to run a programmed sequence automatically. The servos and motor speed controller receive a control signal in the form of Pulse Width Modulation (PWM) digital commands from the Arduino board and are calibrated to output precise blade angle of attack and exact rotor RPM. The Arduino set up is shown in Figure 2.12.

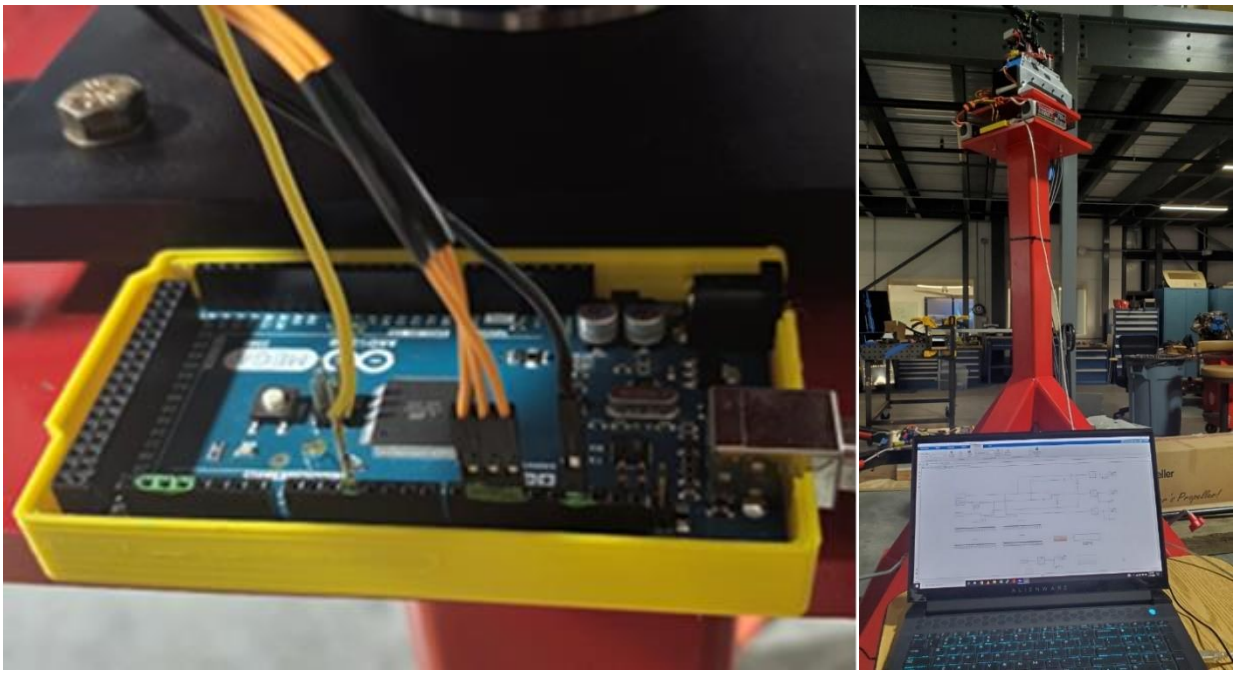

Figure 2.12 Arduino Mega board mounted on Test Stand

Figure 2.13 shows the Simulink block diagram used to control RPM and collective pitch. A sequence can be programmed, for example, to perform a collective pitch sweep in 2-degree increments, from 0 to 13 degrees. This type of test could be performed at any specific RPM.

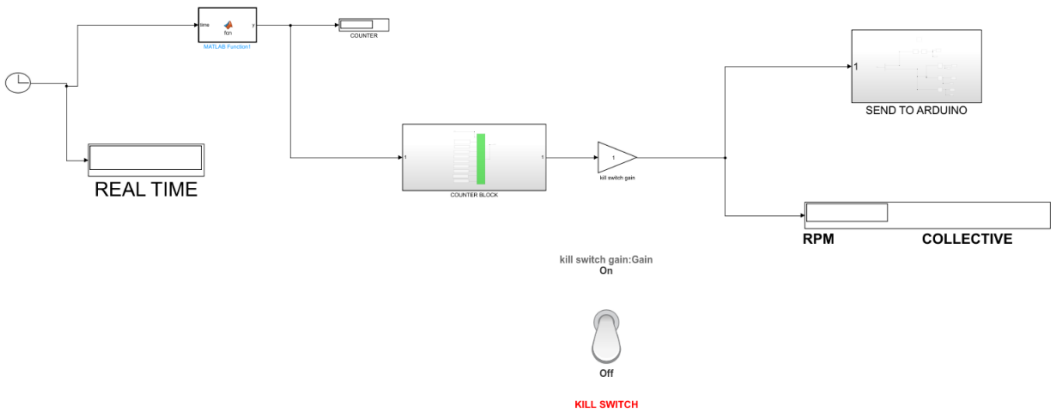

Figure 2.13 Simulink-Arduino Implementation

Two killswitches are implemented on the RTS. One killswitch cuts the signal through Simulink and the other killswitch closes the electrical system with a relay as shown in Figure 2.14.

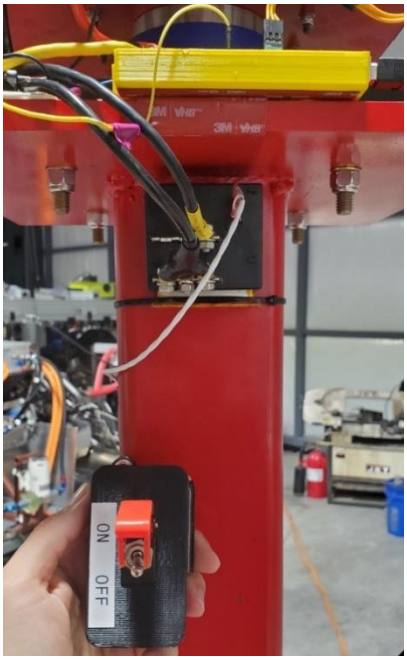

Figure 2.14 Relay Killswitch

Thrust and torque values were taken while running the rotor at collective pitch intervals between 0° and 13° at different RPM. Figure 2.15 shows the axis system for the single DEP pod used to analyze the data.

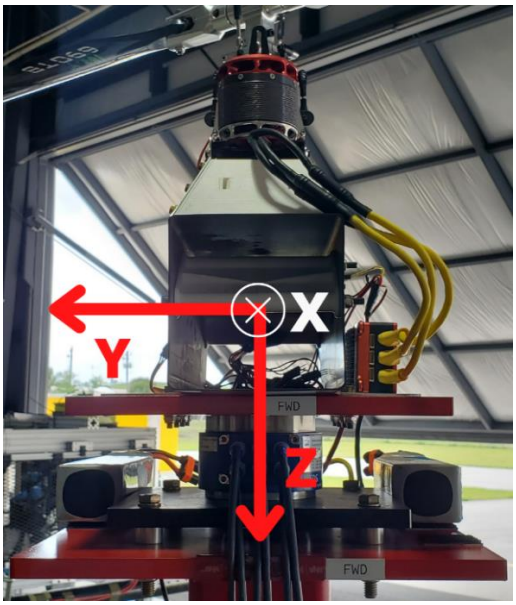

Figure 2.15 DEP unit axis system

For data post-processing and analysis, a Fast Fourier Transform (FFT) with a Butterworth filtering code was developed to isolate the frequencies of interest while removing unwanted noise and vibrations (for example the Load Cell was able to record the vibrations from the electric motor and from the test stand). The plot on top of Figure 2.16 shows the raw data for the force in the X direction collected from the Load Cell during a collective sweep test at 1600 RPM, and the bottom plot of the same figure shows the FFT performed on the data. Figure 2.17 shows the same for the force in the Z direction (Thrust). As expected, the biggest vibration is picked up in the X axis, as can be seen by the high peaks in the FFT of Figure 2.16 against the very low peaks of the FFT performed on the Thrust measurements, shown in Figure 2.17

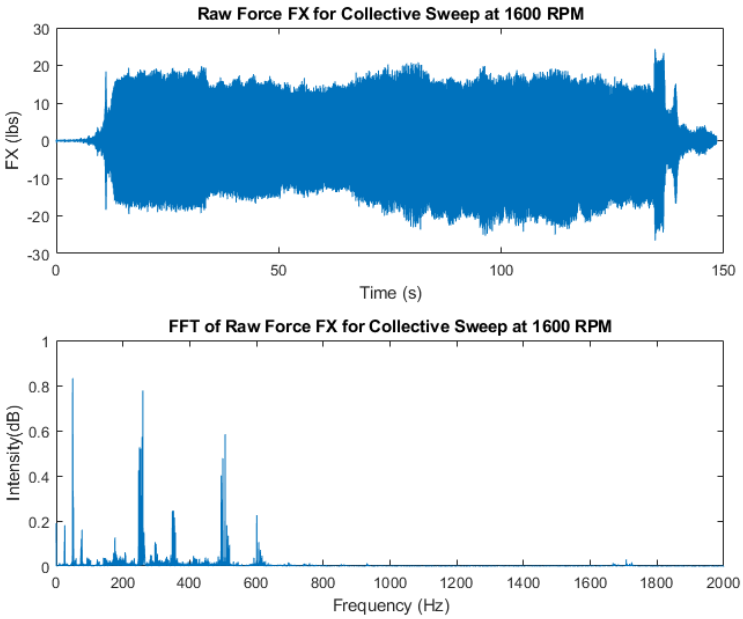

Figure 2.16 Raw force in X direction and FFT plot

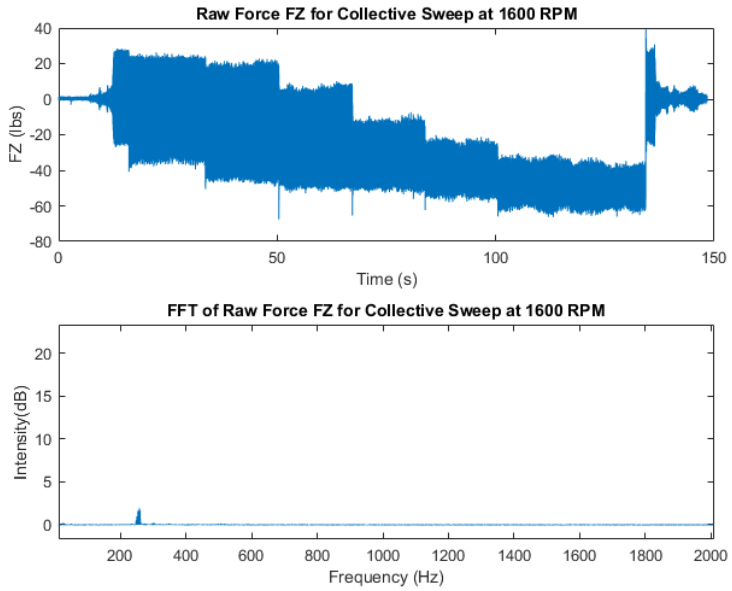

Figure 2.17 Raw force in Z direction and FFT plot

After filtering the data, clear thrust and moment increments can be seen. Figure 2.18 shows the thrust data from the collective sweep test at 1600 RPM. The raw data is shown in blue, and

the filtered data is shown in red. The green dot shows the maximum thrust generated at 1600 RPM with 13° of collective pitch.

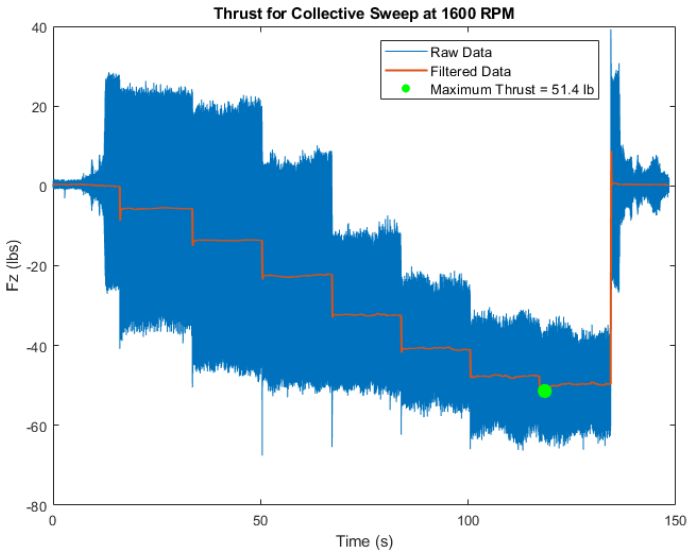

Figure 2.18 Thrust for collective sweep at 1600 RPM

Similarly to Figure 2.18, torque for the collective sweep at 1600 RPM is shown in Figure 2.19

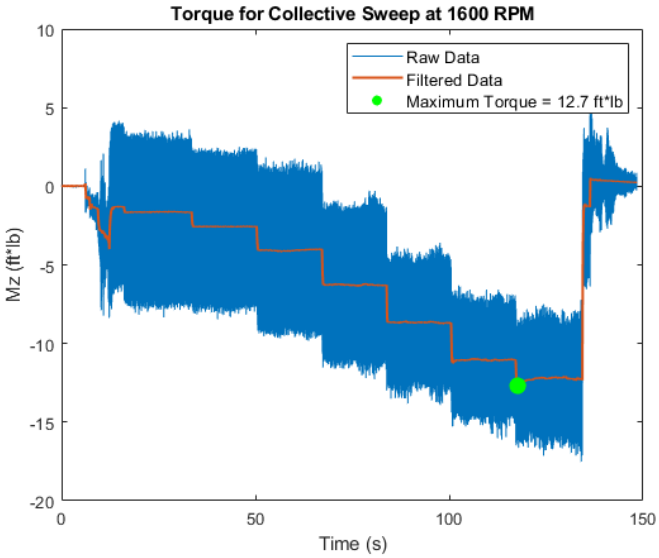

Figure 2.19 Torque for collective sweep at 1600 RPM

After applying the filter, Figure 2.20 shows the final result for the filtered thrust without the raw data and Figure 2.21 shows the final result for the filtered torque for the same sample test case. By looking at the filtered data, each collective pitch step can be easily identified.

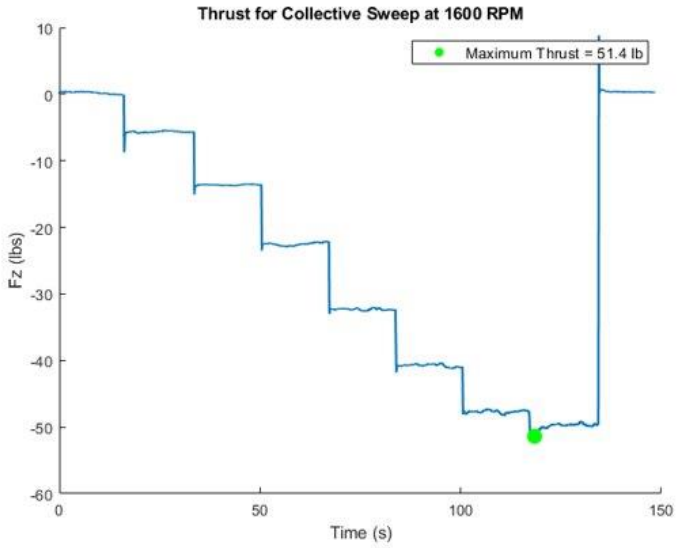

Figure 2.20 Filtered Thrust for collective sweep at 1600 RPM

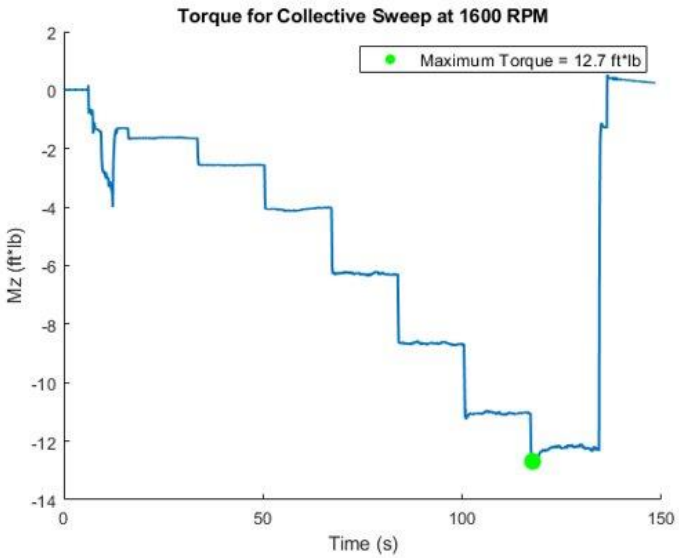

Figure 2.21 Filtered Torque for collective sweep at 1600 RPM

The same filter used for the data presented above was used to filter all the data acquired from experimental tests.

2.4 Closed Form Equation Derivation

After careful analysis of the simulation and experimental results, it became of interest to propose a closed form equation that could show similar trends to obtain quick results for the power required from a rotor in hover. Starting from Equation 5-8 on page 112 from McCormick's "Aerodynamics of V/STOL Flight" [36] assuming uniform inflow and neglecting viscous effects, the total power coefficient can be written as the sum of the induced and profile power coefficients:

$$C_P = C_{Pi} + C_{Pp} \approx \frac{C_T^{\frac{3}{2}}}{\sqrt{2}} + \frac{\sigma \overline{C_D}}{8} \tag{2.6}$$

McCormick shows that for a rectangular blade the mean drag coefficient $\overline{C_D}$ can be related to the mean lift coefficient of a rotor with the following equation:

$$\overline{C_D} = C_{d0} + k\overline{C_L^2} \tag{2.7}$$

For preliminary calculations, typical values for C_{d0} range between 0.008 and 0.011 as shown by NACA [37], Leishman [24], and McCormick [38]. k is a constant that depends on the blade planform [36].

The mean lift coefficient for a rotor can be written as:

$$\overline{C_L} = 6\frac{C_T}{\sigma} \tag{2.8}$$

Where C_T is the thrust coefficient:

$$C_T = \frac{T}{\rho A V_{Tip}^2} \tag{2.9}$$

σ is the rotor Solidity:

$$\sigma = \frac{N_b c R}{A}$$

Where:

- N_b is the number of blades.
- k is a constant determined by the blade planform.
- T is the hover thrust, that can be assumed to be equal to the weight of the helicopter.
- ρ is the density.
- c is the blade chord.
- C_{d0} is the profile drag coefficient at zero lift (shown in McCormick as δ0 [36]).
- R is the radius.
- A is the area of the rotor disk.
- The tip speed is:

$$V_{Tip} = \Omega R$$

- Ω is the rotational speed (rad/s).

Assuming a constant thrust case, the induced power coefficient can be assumed to be constant and the derivation can be focused on the profile power coefficient.

Rewriting the profile power coefficient term of equation 2.6 with the mean drag coefficient from equation 2.7:

$$C_{Pp} = \frac{\sigma C_{d0}}{8} + \frac{\sigma}{8} k \overline{C_L^2}$$

Substituting equation 2.8 in the equation above:

$$C_{Pp} = \frac{\sigma C_{d0}}{8} + \frac{\sigma}{8} k \left(6 \frac{C_T}{\sigma}\right)^2$$

Substituting equation 2.9 in the equation above and simplifying:

$$C_{Pp} = \frac{\sigma C_{d0}}{8} + \frac{\sigma}{8} k \left(\frac{6T}{\sigma \rho A V_{Tip}^2} \right)^2$$

$$C_{Pp} = \frac{\sigma C_{d0}}{8} + \frac{36}{8} \frac{kT^2}{\sigma \rho^2 A^2 V_{Tip}^4}$$

Writing out the solidity term to simplify the equation:

$$C_{Pp} = \frac{N_b c R C_{d0}}{8A} + \frac{36}{8} \frac{kT^2}{N_b c R \rho^2 A V_{Tip}^4}$$

Writing the profile power from the coefficient form, multiplying by the density, area and tip speed cubed and simplifying, leads to the final result for the profile power:

$$P_{Profile} = \frac{\rho V_{Tip}^3 N_b c R C_{d0}}{8} + \frac{36}{8} \frac{kT^2}{N_b c R \rho V_{Tip}} \tag{2.10}$$

Similarly the induced power can be extracted from the induced power coefficient, which leads to the final formulation for the total power for a rotor in hover as a function of tip speed:

$$P_{Total} = P_{Induced} + P_{Profile} = \frac{1}{\sqrt{2}} \left(\frac{T}{\rho A V_{tip}^2} \right)^{\frac{3}{2}} \rho A V_{tip}^3 + \frac{\rho V_{Tip}^3 N_b c R C_{d0}}{8} + \frac{36}{8} \frac{kT^2}{N_b c R \rho V_{Tip}} \tag{2.11}$$

Tip speed and RPM can be interchanged in the equation above with the following formula:

$$V_{Tip} = \frac{2\pi R}{60} RPM$$

Leishman [24] includes an additional induced power correction factor in the induced power term. This factor is derived from rotor measurements and it accounts for non-ideal effects on the blade such as nonuniform inflow over the blade, and tip loss. Leishman [24] estimates a typical average induced power factor to be 1.15. Including the induced power correction factor in equation 2.11 as k_0, the equation for the total power of a rotor in hover can be written as:

$$P_{Total} = P_{Induced} + P_{Profile} = \frac{k_0}{\sqrt{2}}\left(\frac{T}{\rho A V_{tip}^2}\right)^{\frac{3}{2}} \rho A V_{tip}^3 + \frac{\rho V_{Tip}^3 N_b c R C_{d0}}{8} + \frac{36}{8}\frac{kT^2}{N_b c R \rho V_{Tip}} \quad (2.12)$$

Equation 2.12, can be easily derived by expanding and writing out every term that comprises equation 2.6 as shown above. On page 112, McCormick [36] presents the same equation in coefficient form, without writing out the terms with their respective components and without including the induced power correction factor explained by Leishman [24].

For a known rotor geometry and test conditions, only three unknowns are left in equation 2.12: k_0, C_{d0}, and k. To maximize the accuracy of the power predicted with equation 2.12, these three values can be obtained from a simple curve fit done to match the predicted power output from the equation with the results from simulation or experimental tests. For example, the curve fit done for the Goblin rotor analyzed in this research generated the following results: C_{d0}= 0.008, $k_0 = 1.1$, and $k = 0.03$.

3 Results and Discussion

This section will present results from the 3 different methods explained in the methodology: results from simulation (MATLAB code with BEMT, Xfoil and WOPWOP), results from the RTS tests, and results from the closed form equation proposed. The results will all be compared at different constant thrust cases.

3.1 Simulation Validation

The first results presented in this section are used to compare and validate the simulation results with the experimental results obtained from the RTS. Both the simulation and experimental results were obtained from testing a single 2-bladed rotor capable of RPM and collective pitch control equipped with the Goblin blade, a rectangular untapered blade used on the full scale drones built at the EFRC. The rotor characteristics and blade planform are described in Table 3.1 below:

Table 3.1 Geometry of rotor equipped with Goblin blade.

Blade Radius	2.5417 ft.
Blade Chord	0.2083 ft.
Blade Airfoil	NACA 0015
Number of Blades	2

Figure 3.1 (A) shows a picture of the physical Goblin blade while Figure 3.1 (B) shows a MATLAB 3-D rendering of the rotor equipped with two Goblin blades.

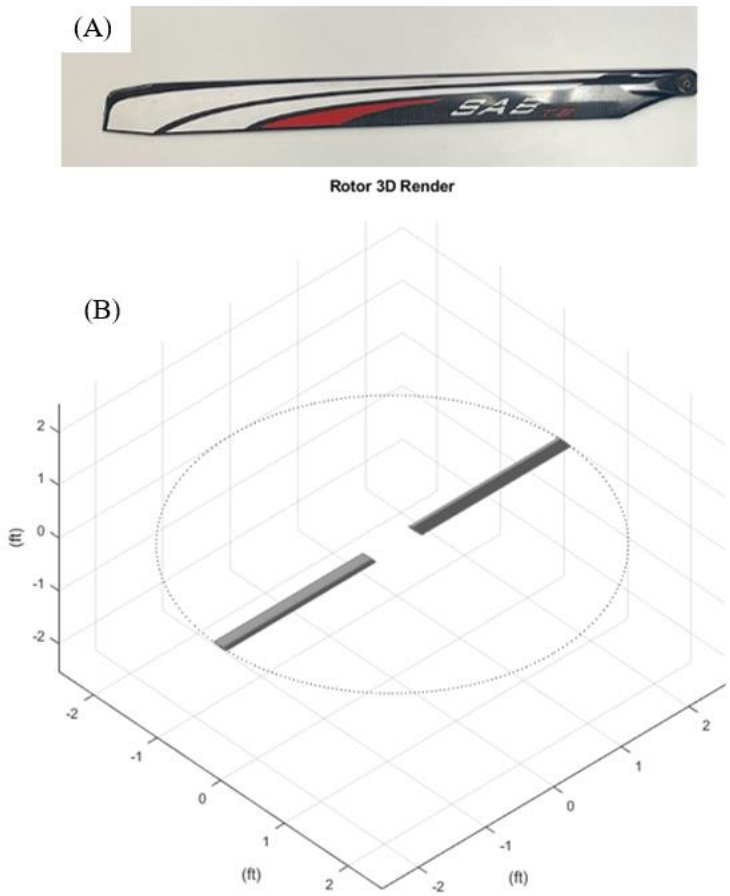

Figure 3.1 Picture of Goblin blade (A). MATLAB 3-D Rendering of rotor with Goblin blades (B).

Figure 3.2 below shows a comparison of power required at a certain combination of collective pitch and RPM for the Goblin rotor. The RPM ranges from 1000 to 1800, with a tip Mach number of 0.23 to 0.42, while the Collective is tested at the following points: 2°, 4°, 6°, 8°, 10°, 12°, and 13°.

The lines are the values predicted from the simulation and the single dots are the color-coded results obtained from experiments. The power obtained from experiments is matched very accurately from the MATLAB simulation as shown by the experimental values (shown with dots) falling exactly on the same constant collective lines in the graph.

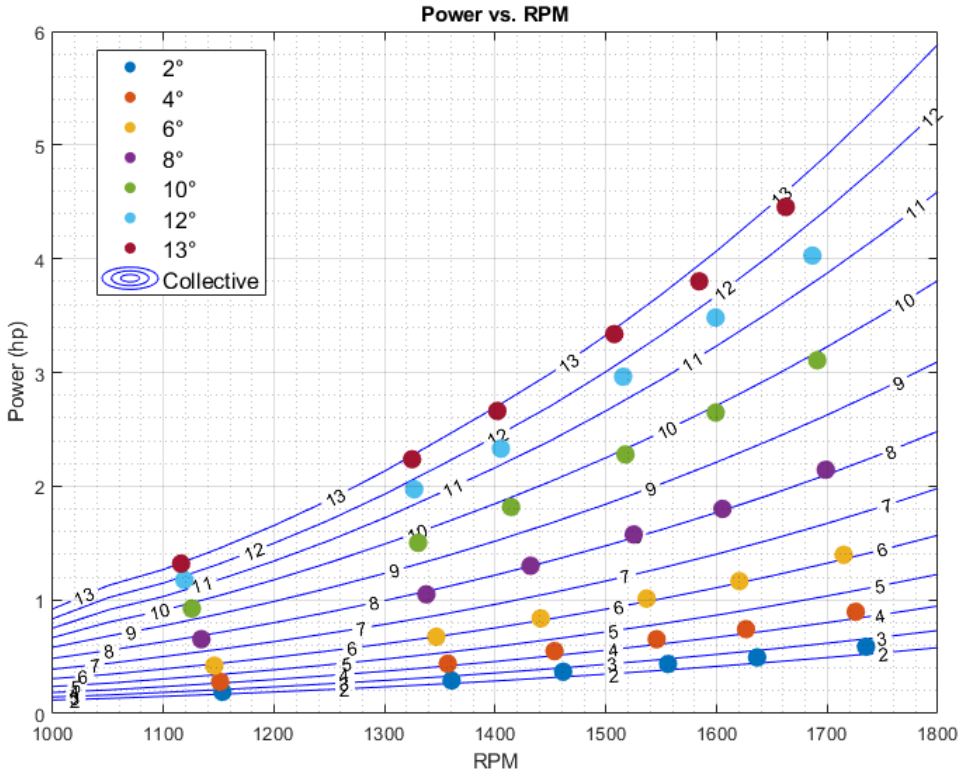

Figure 3.2 RPM vs Power – code & experimental values

Figure 3.3 shows a comparison of thrust produced at a certain combination of collective pitch and RPM. It can be noticed from the figure, that the code predicts the generated thrust accurately.

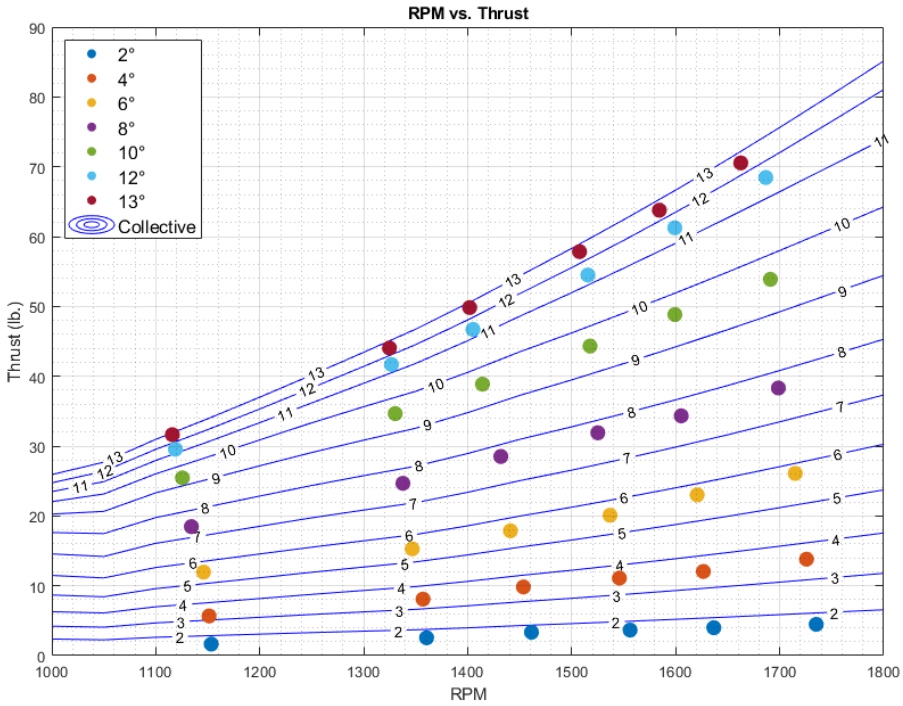

Figure 3.3 RPM vs Thrust – code & experimental values

The small differences could be caused from the fact that the RTS collective pitch deflections are calibrated manually and there is a known tolerance of about ± 0.1° to ± 0.3° for every collective pitch deflection as well as from the fact that the stand experiences very high vibrations especially at such high collective angles, where the loads on the blades are high. There could be the possibility that some thrust in the vertical direction is lost to lateral force contributions if the stand becomes unleveled during tests from the high vibrations. In addition, the arms of the rotorhead on the RTS have a small margin of rotation where if a force is applied on them even while Simulink is sending a defined collective pitch, the arms can slightly be rotated thus changing the pitch of the blades. It could be speculated that at high collective deflections past 8°, the high loading on the blades could be overpowering the servos that are commanding a set collective pitch, thus slightly changing the effecting pitch of the rotating blades. Including servos

with live telemetry of their arm angle position will be the subject of future work. These small differences do not change the overall trend of the results; they merely slightly affect the magnitude.

3.2 Simulation Results

The simulation results presented in this section were obtained by simulating the performance and noise results of the Goblin rotor at several combinations of RPM and Collective pitch. The RPM ranges from 1000 to 2000 with a step interval of 50 RPM, while the Collective pitch ranges from 1° to 18°, with 1° step interval.

For this research it was of interest to compare the noise and power required for the rotor at different constant thrust conditions. The constant thrust values were picked to resemble the actual thrust produced by the rotor during physical flights of the drones built at the EFRC and they range from 40 lb. to 80 lb. depending on the different mission profiles. Figure 3.4 below shows how different combinations of operating RPM and collective pitch on the blade can be utilized to maintain the same constant thrust. However, while the thrust is maintained constant, the power required to operate the rotor increases significantly as the collective pitch of the blades is increased, even though the operating RPM is decreased.

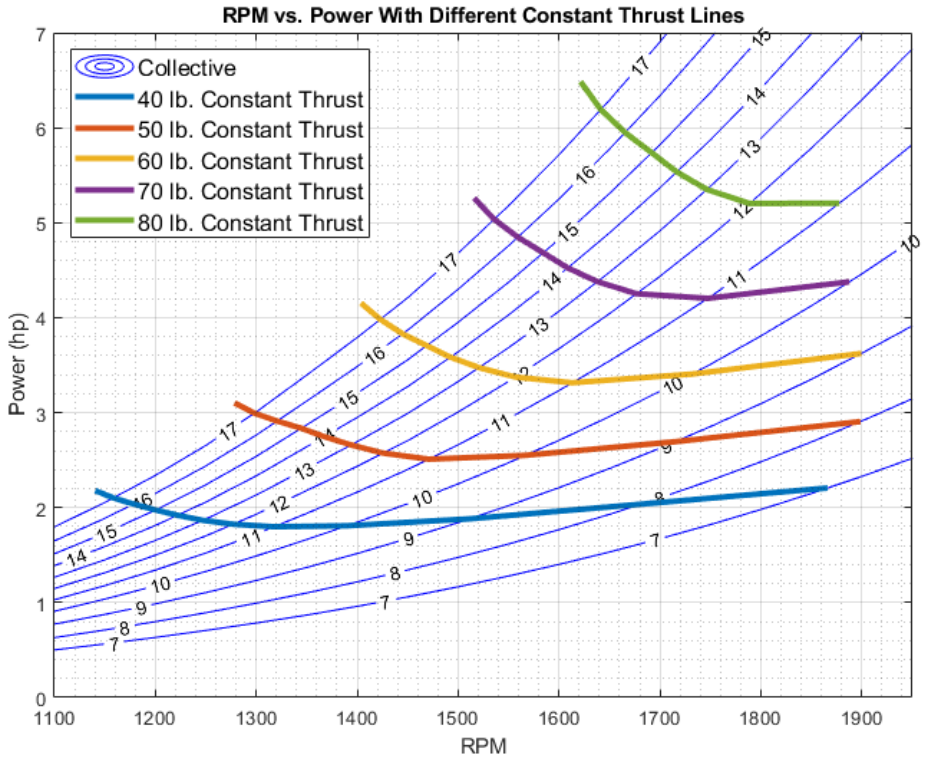

Figure 3.4 RPM vs Power required at different constant thrusts

To illustrate the reason behind the behavior of the constant thrust lines shown above, 2 cases will be shown in detail: the 40 lb. and 60 lb. constant thrust cases. Figure 3.5 below shows the 40 lb. constant thrust case. By looking at the figure it becomes obvious that there is a single best operating point where producing 40 lb. of thrust takes the least amount of power. This ideal operating point is indicated by the red dot in the figure and it happens at an operating RPM of 1318 with 11° of collective pitch.

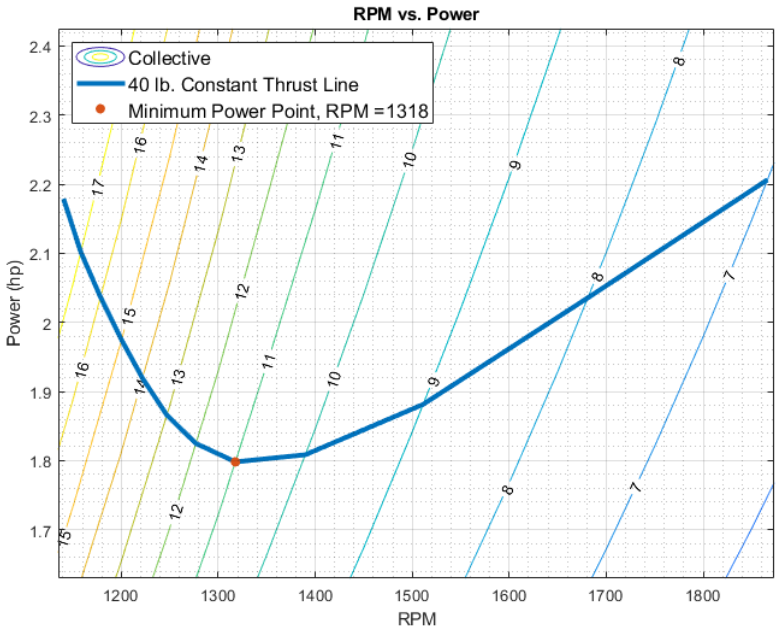

Figure 3.5 RPM vs Power with Constant 40 lb. thrust line and minimum power point

Figure 3.6 presents the lift to drag ratio (L/D) at different positions along the blade shown as a percentage of the radius (55%, 65%, 75% and 80%). The L/D values at these stations are obtained for each combination of RPM and collective pitch from Figure 3.5. When the blade is operated at 1318 RPM and 11° of collective pitch, where the minimum power point is reached, all the different sections of the blade are shown to operate at the highest L/D when compared to the other RPM and Collective pitch combinations used to obtain the same 40 lb. of constant thrust.

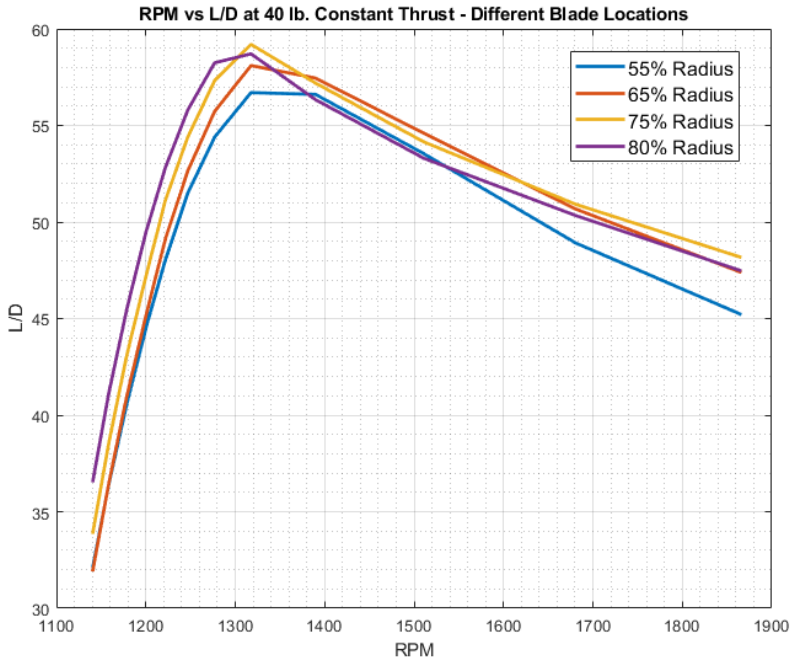

Figure 3.6 RPM vs L/D for the 40 lb. constant thrust case at different radial stations

The same behavior can be seen when looking at a 60 lb. constant thrust case as shown in Figure 3.7. The best operating RPM here is 1613 also at 11° of collective pitch.

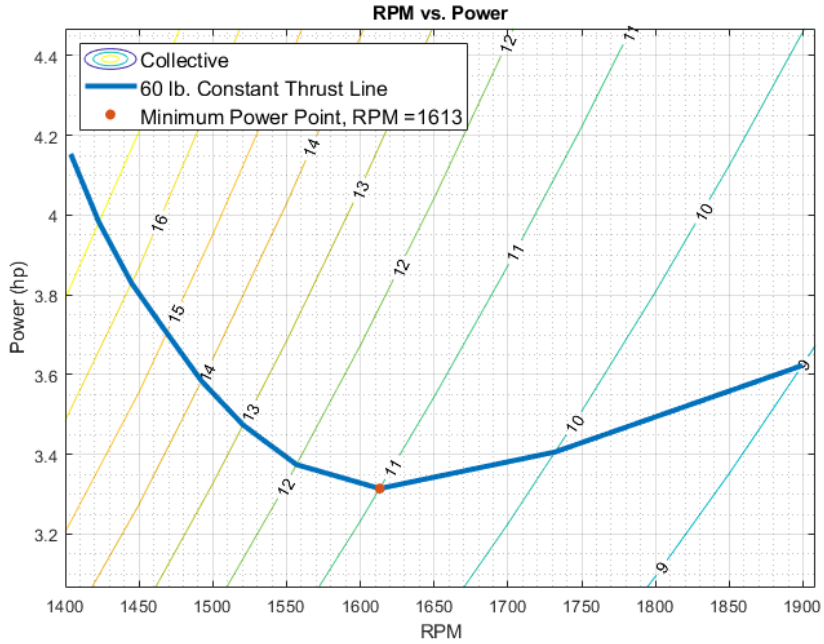

Figure 3.7 RPM vs Power with Constant 60 lb. thrust line and minimum power point

For the 60 lb. constant thrust case, when looking at Figure 3.8, it can be seen that most of the blade sections operate at the highest L/D when spinning at 1613 RPM with 11° of collective pitch. The 80% radius location seems to have a higher L/D at a lower operating RPM but the effect is small when the rest of the blade has the highest L/D at the same RPM.

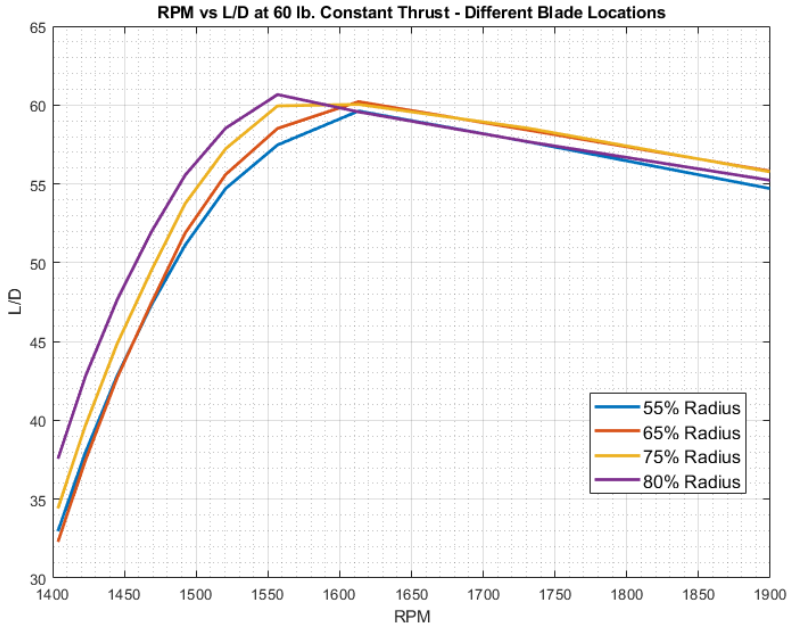

Figure 3.8 RPM vs L/D for the 40 lb. constant thrust case

Knowing the operating point for minimum power, the minimum noise point is calculated next. The noise results obtained from WOPWOP are presented for the same operating conditions and constant thrust cases. The observer is placed in plane with the rotor at a distance of 50 ft. away. In the methodology section it was stated how when analyzing a constant thrust condition with a fixed observer, a decrease in RPM will lead to a decrease in both the thickness and loading noise contributions. Figure 3.9 presents noise contours obtained with WOPWOP from the same constant thrust cases shown in Figure 3.4.

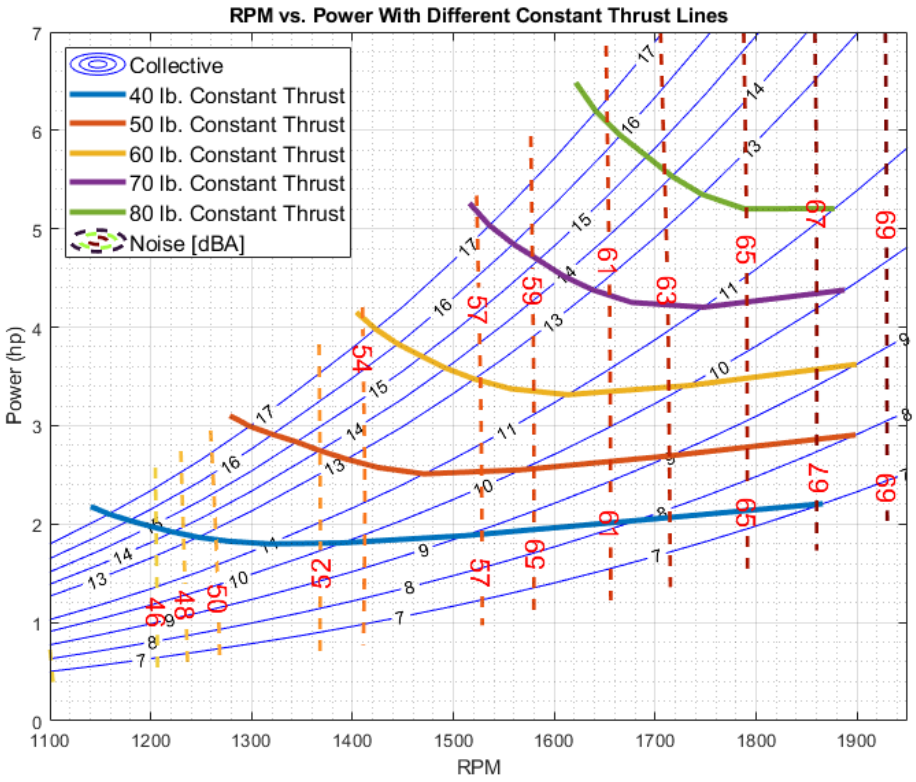

Figure 3.9 RPM vs Power required at different constant thrusts with Noise contours

Figure 3.9 confirms what was previously concluded from Figure 2.4: a decrease in RPM will lead to a decrease in loading and thickness noise contributions. For example, when following the 50 lb. constant thrust line shown in orange, it can be seen how a decrease in RPM will decrease the noise from 69 dBA to 50 dBA, while the power required reaches a minimum and then increases with increasing collective pitch. Figure 3.9 already shows that the minimum power and minimum noise points do not occur at the same operating conditions (RPM and collective pitch). Noise results are now presented for the same 40 lb. and 60 lb. constant thrust cases presented before. Figure 3.10 shows the power required to maintain 40 lb. of constant thrust (in black) and it also shows the noise (in red) produced at each operating point that produces the 40 lb. of thrust. The evaluated points are also clearly shown in the figure.

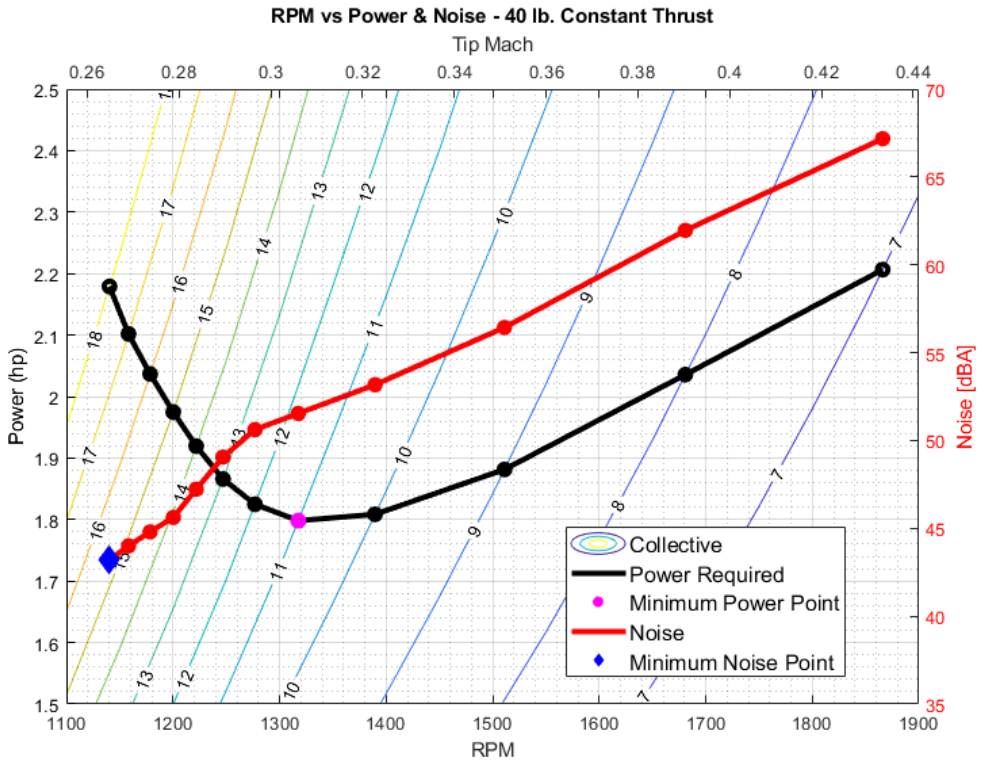

Figure 3.10 RPM vs Power and Noise for 40 lb. Constant Thrust

The minimum power point is shown with a purple circle, while the minimum noise point is shown with a blue diamond in Figure 3.10.

Figure 3.11 shows the same results as Figure 3.10, with the addition of the loading and thickness noise components. The loading noise component is shown in green and the thickness noise component is shown in blue.

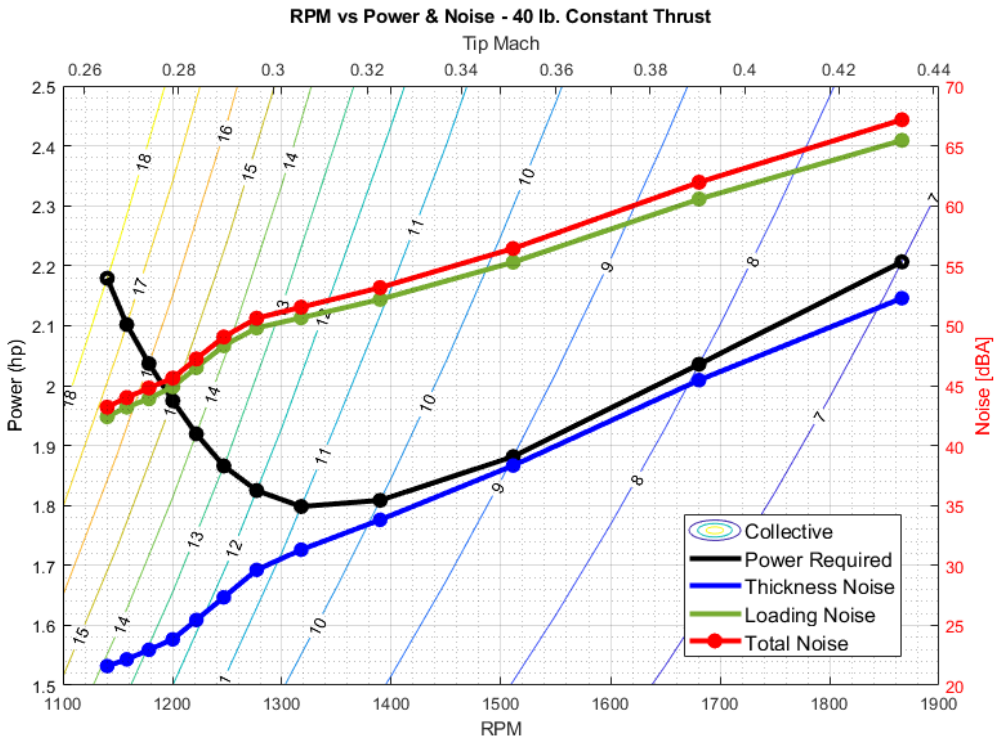

Figure 3.11 RPM vs. Power and Noise for 40 lb. Constant Thrust – with Loading & Thickness noise contributions

The power required and noise emission results for the 60 lb. of constant thrust case are shown in Figure 3.12 below.

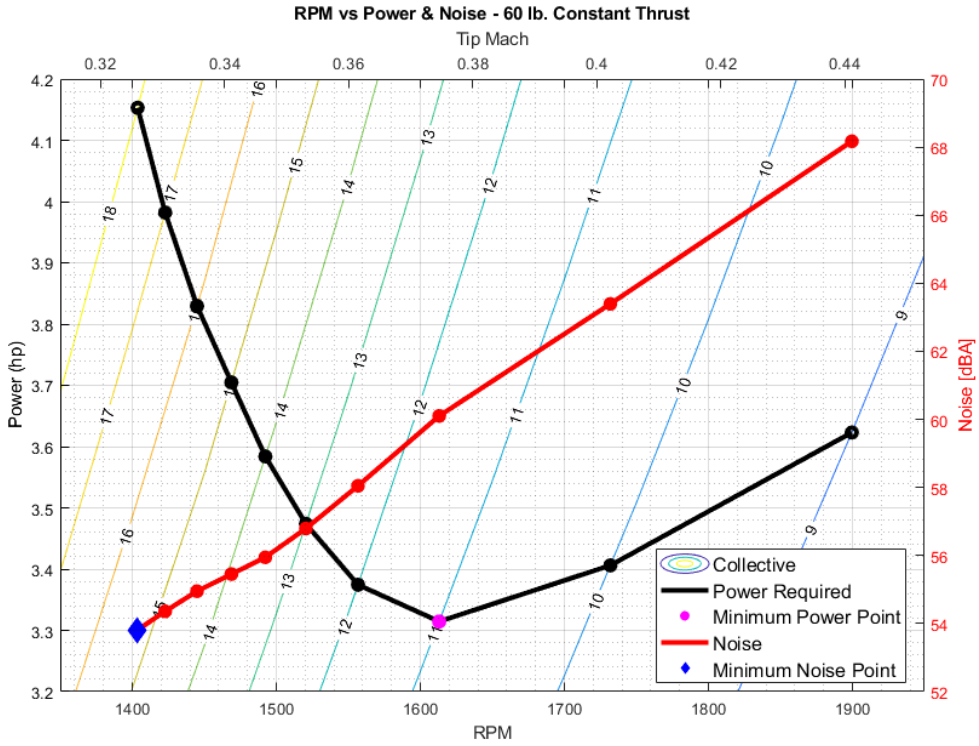

Figure 3.12 RPM vs Power and Noise for 60 lb. Constant Thrust

Figure 3.13 presents the loading and thickness noise components for the 60 lb. of constant thrust case.

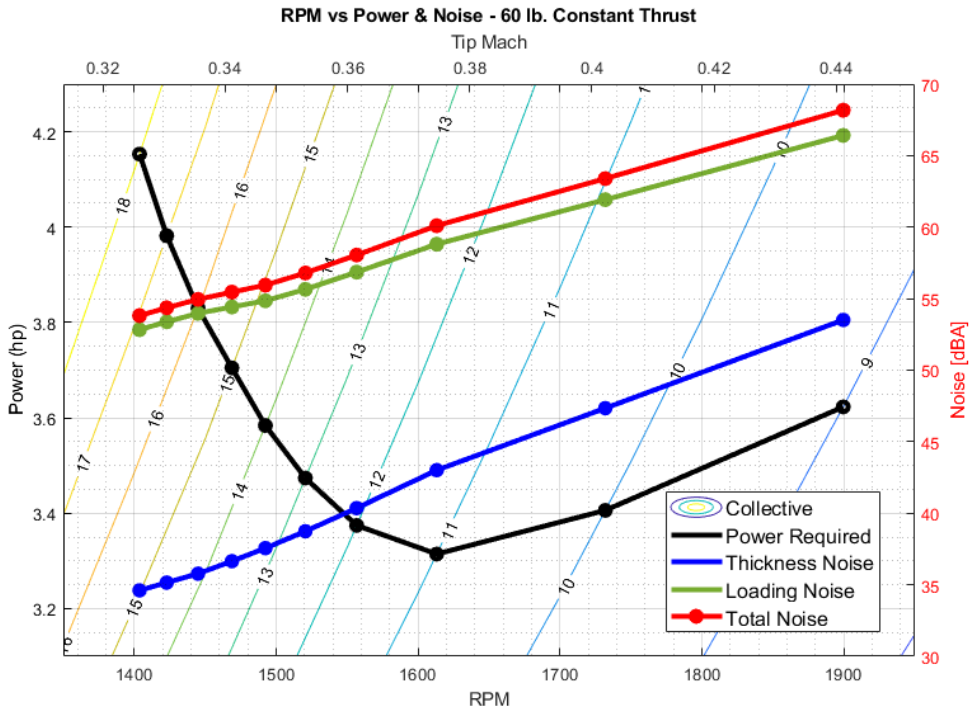

Figure 3.13 RPM vs. Power and Noise for 60 lb. Constant Thrust – with Loading & Thickness noise contributions

By looking at Figure 3.10 and Figure 3.12 it becomes obvious that minimum power and minimum noise are reached at two very distinct points, characterized by two different operating conditions, defined by two distinct RPM and collective pitch combinations. In addition the figures show that it takes more power to be quiet. In other words, RPM or tip speed is the main factor that will affect rotor noise from thickness and loading contributions, therefore to decrease noise, the operating RPM must be reduced, as shown by the red line in Figure 3.10 and Figure 3.12. However, to maintain the same constant thrust for a hover condition, the collective pitch of the blades has to be increased while the RPM is decreased. This will cause an increase in the power required from the rotor.

Figure 3.11 and Figure 3.13 show how loading and thickness noise decrease with decreasing tip Mach number, following the same trend presented in Figure 2.4. As expected, with the

maximum tip Mach number being 0.44, loading noise is the dominant noise contribution, as also confirmed by Figure 2.4.

The relationship between noise and power required at constant thrust is really important for AAM vehicles as an algorithm could be developed that switches the vehicle's operating mode from high efficiency, high noise, to low noise, low efficiency depending on where the vehicle is located during its mission profile. As also stated by Gartenberg [22], when the vehicle is flying over the ocean, or over undeveloped land, where noise is not a concern, the vehicle can operate in its high efficiency (minimum power required), high noise point. However, when the vehicle is operating in an urban environment, where noise is a concern, the vehicle can now switch to its low noise operating point, thus increasing the power required, which as shown in this analysis increases dramatically to a maximum, as noise decreases to a minimum.

3.3 Experimental Results

The RTS was used to test the Goblin blades to see if similar results to the simulation could be obtained with experimental tests. Figure 3.14 shows the power vs. RPM results normalized for standard sea level conditions for the 2 bladed rotor with Goblin blades at different constant thrust conditions. The black dots indicate the actual values obtained from testing that have been filtered and post-processed in MATLAB to give clearer results.

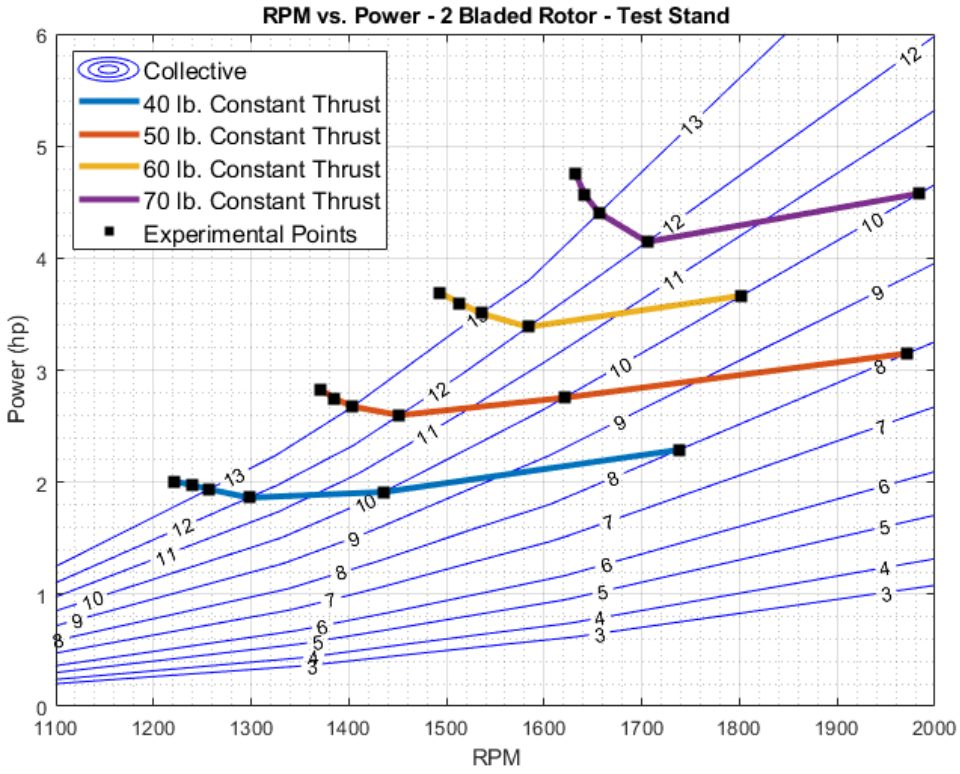

Figure 3.14 RPM vs Power required at different constant thrusts – 2 Bladed Rotor with Goblin Blades - RTS results

Figure 3.14 shows that there is an increase in power required to maintain constant thrust while lowering RPM and increasing collective pitch. More importantly the figure shows that there is an optimum point, where if the blade is operated at a very specific RPM and collective pitch, the power required will be at a minimum. Moving from that minimum point in either direction, toward the right of the graph by increasing RPM and decreasing collective, or toward the left of the graph by decreasing RPM and increasing collective, will lead to an increase in power required.

From the experimental and the simulation results it can also be seen that the power required to hold constant thrust by decreasing RPM and increasing collective pitch, increases more rapidly and more aggressively when compared to the power required by increasing RPM and

decreasing collective. This is expected because the rotor is operating at high angles of attack, where drag increases quickly thus requiring more torque and therefore more power to be delivered to the rotor. In addition parts of the blade could be operating at or near stall conditions.

An important conclusion can be drawn from the experimental tests: the power required while holding constant thrust maintains the same U-shaped trend found in the simulation where a best operating condition can be found that minimizes the power required. Combining this trend with the fact that noise decreases with decreasing RPM, for a constant thrust case, it can be concluded that the operating point at which noise reaches a minimum is not the same operating point where power reaches a minimum. There are 2 distinct RPM and Collective combinations where if noise is minimized, power is increased, or if power is minimized, noise is increased.

Figure 3.15 below presents a combined plot for the power required at different constant thrust values for both the experimental and simulation results. As expected from the validation section 3.1, where the simulation results were successfully validated with the experimental tests, Figure 3.15 shows that the constant thrust lines obtained from the simulation (shown with dashed lines) agree accurately with the experimental constant thrust lines (shown with solid lines) confirming the accuracy of the simulation predictive capabilities.

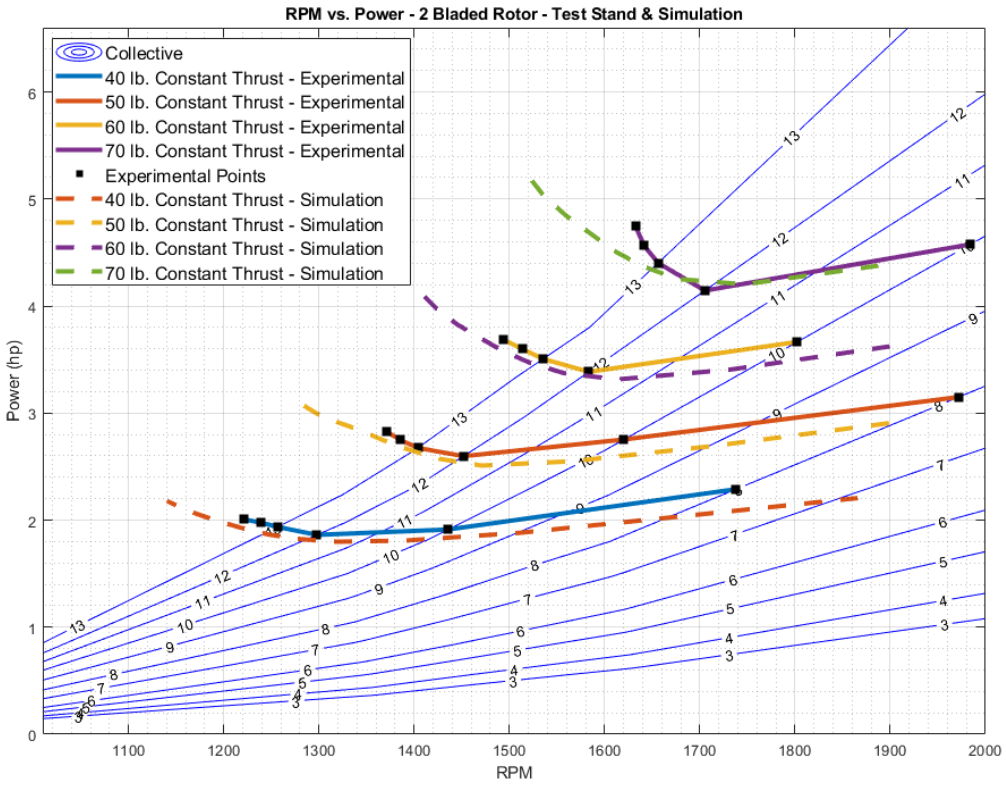

Figure 3.15 RPM vs Power required at different constant thrusts – 2 Bladed Rotor with Goblin Blades – Experimental & Simulation Results

3.4 Closed-Form Equation Results

The power predicted from equation 2.12 derived previously is analyzed in this section and compared to the results from simulation and experiments. The coefficients, obtained from a curve fit with experimental and simulation results, used in equation 2.12 are: C_{d0}= 0.008, $k_0 =$ 1.1, and $k = 0.03$. The predictive capabilities of the equation can first be proven when comparing its results for the power required to the results obtained from the MATLAB code simulation for the 2 bladed Goblin rotor at different constant collective pitch angles, for a different range of RPM as shown in Figure 3.16.

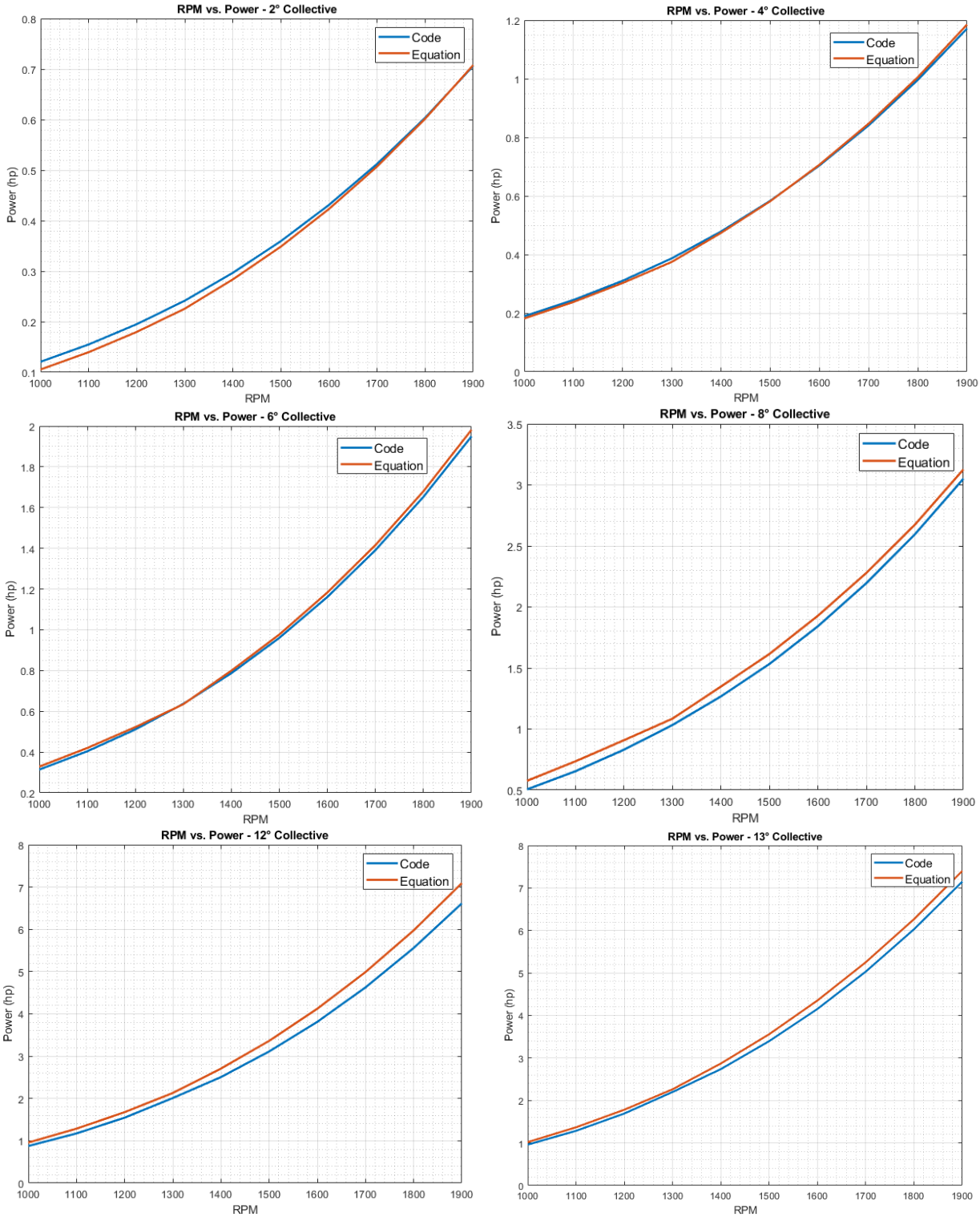

Figure 3.16 RPM vs Power at different constant collective pitch – Comparison between Simulation code and Derived Equation

The power predicted from the code (shown in blue) and the power predicted from the equation (shown in red) show very good agreement and the curves almost overlap. Figure 3.17 shows the power required predicted with the derived equation for a constant thrust of 40 lb. for different operating RPM. It is hidden in the equation that, as mentioned previously, the decrease in RPM at constant thrust, needs an increase in collective pitch. Even though the equation does not predict what collective pitch will be needed to generate the required constant thrust, it does show the same trend presented in the MATLAB simulation and RTS experiments, where power reaches a minimum and increases with decreasing RPM and increasing collective pitch or increasing RPM and decreasing collective pitch.

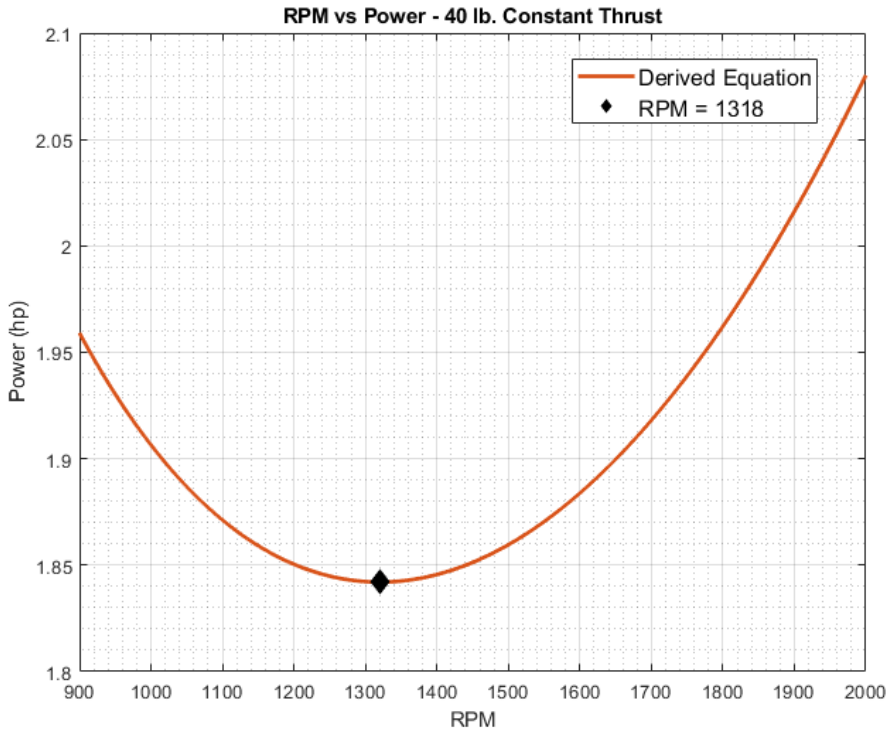

Figure 3.17 RPM vs Power for 40 lb. constant thrust – Derived Equation

Taking the derivative of the derived equation will lead to finding the best operating RPM, where the power required is at a minimum, as shown with the black diamond.

Figure 3.18 shows the combined results from the RTS (in yellow), from the MATLAB code (in blue) and from the derived equation (in orange) for a constant thrust case of 40 lb. The minimum power points are shown with diamonds as labeled in the figure.

When compared to the experimental results, the simulation shows an error percentage of 3.2% which confirms the accuracy of the MATLAB code used. The rapid increase in power when moving away from the minimum power point is also captured accurately by the simulation.

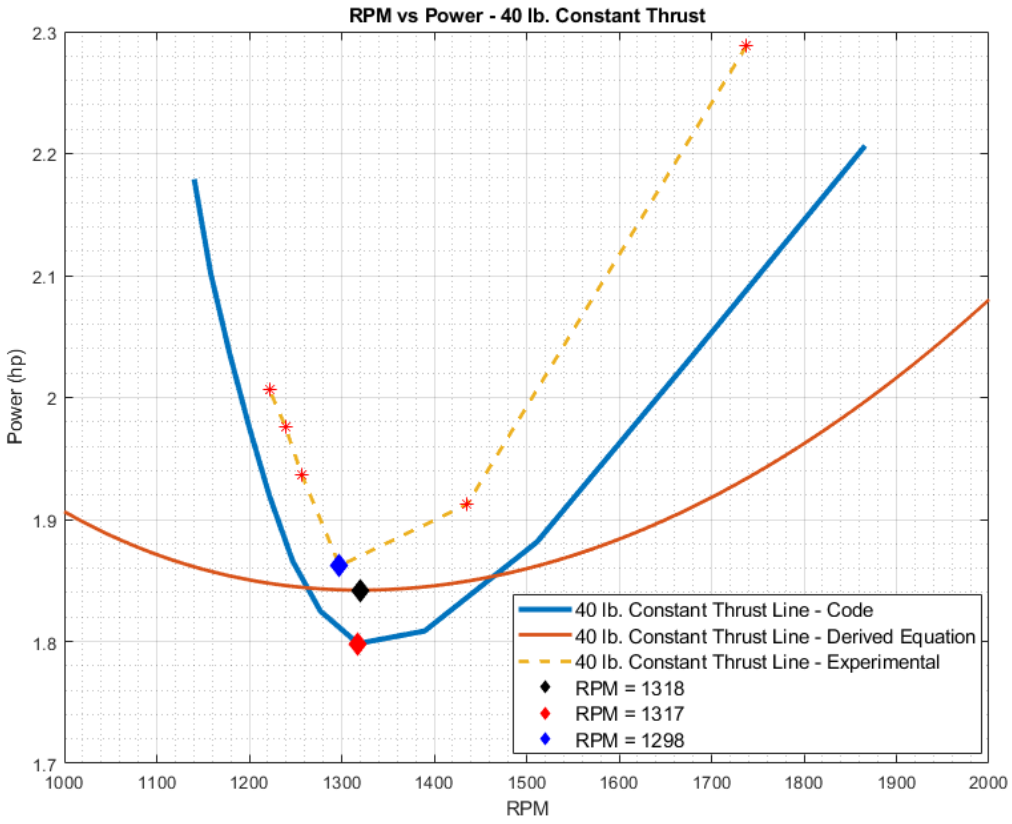

Figure 3.18 RPM vs Power for a 40 lb. constant thrust case – results from MATLAB code (blue), RTS experimental tests (yellow) and derived equation (orange)

Figure 3.18 shows the predictive capability of the derived equation as it predicts the minimum power point with only a 2% error when compared to either the simulation or experimental results. Even though the derived equation can accurately predict the minimum power point, it cannot accurately predict the high increase in drag with increasing collective or increasing RPM that drives the increase in power shown in the simulation and experimental results. This difference proves the importance of using the simulation to study the behavior of a rotor at constant thrust, but the equation shows that in a matter of seconds, the best operating RPM can be obtained for a user-defined rotor, and the minimum power point is predicted very accurately without having to run simulations for extended periods of time spanning one to two days. As decreasing RPM will decrease noise, this operating point will minimize power while emitting the lowest possible noise for operation at the minimum power point. As shown in the previous sections, the absolute minimum noise point will require a high increase in power to hold the desired constant thrust.

4 Conclusion

This research focused on the noise and power relationship for a rotor/propeller equipped with rectangular blades at constant thrust. A rotor test stand has been designed and built to carry out physical tests of a rotor equipped with rectangular blades. A MATLAB algorithm has been developed and integrated with Xfoil and WOPWOP to perform performance and noise analysis of a rotor in a hover condition. The hardware results have been used to validate the simulation. It has been stated and proven that noise, from thickness and loading contributions, decreases with decreasing RPM, while holding constant thrust by increasing blade collective pitch. Simulation and experimental results have been used to show that for a variable pitch rotor/propeller equipped with an electric motor, the minimum noise and minimum power points for any constant thrust case are not the same and they are achieved at two very distinct operating points defined by a specific RPM and collective pitch setting. It has been shown that in order to minimize noise from loading and thickness contributions, power increases, and in order to minimize power, noise increases. It has been shown that there is a best operating point, where power required to hover reaches its minimum, and moving from that point either by increasing RPM and decreasing collective, or by decreasing RPM and increasing collective leads to an increase in power required. The minimum power point is reached by operating the blade at its best lift to drag ratio for the required hover thrust within the feasible RPM and collective pitch ranges. In the end a closed form equation has been proposed that can be used to estimate the power required for a rotor at constant thrust as a function of RPM or tip speed. Taking the derivative of the derived equation can be used to quickly find the best operating RPM that minimizes the power required for a rotor at constant thrust and it could be used in the preliminary rotor or propeller design cycle analysis.

4.1 Limitations

The most important limitation of the results presented in this document is the fact that broadband noise has not been included in the analysis. While thickness and loading noise have been shown to decrease with RPM regardless of blade pitch, it is expected that a point can be reached where the collective pitch of the blades is high enough to cause flow separation around the blade leading to broadband noise playing an important part in the analysis leading to a possible increase in noise even though the operating RPM keeps decreasing as shown in Figure 2.4. This limitation will be part of future work.

As mentioned by Santacruz [23], the aerodynamic analysis of the blades performed with the BEMT and Xfoil assumes that the flow is subcritical, and it is therefore a predictive limitation, as the rotor tip speed must remain subcritical, which is usually the case for eVTOLs. Another limitation is that Xfoil does not provide results after stall, and the code will crash past this point. It is imperative for the user to make sure to use the algorithm in regions before stall is reached. For example, the maximum collective pitch angle analyzed for the Goblin rotor is 18°, after which the algorithm crashes as stall is reached.

4.2 Future Work

Future research work should focus on 4 main areas. The first and most important area is adding rotor broadband noise predictive capabilities to the code to investigate how the results are affected.

The second area is upgrading the Rotor Test Stand with live telemetry servos and speed controller to be able to monitor the servo arm deflection angle and power draw in real time; this way the collective pitch angle of the blades can be programmed with 100% accuracy and checked live during tests and the rotor can be tested at higher speeds and higher collective angles

with the guarantee that the rated power for the electric motor will not be exceeded. Upgrades to the RTS should also include a bigger electric motor that will allow for testing of larger rotors. In addition noise testing equipment should be included as part of the RTS testing sequence in order to provide physical noise results for further validation of the code predictive powers.

The third area of interest for future work is to investigate the noise and power relationship in forward flight for a propeller or a rotor. This could also translate to an additional upgrade for the RTS, allowing for mounting of a DEP pod to simulate a forward flight scenario.

The fourth and last area of interest for possible future work would focus on investigating how taper, twist and chord affect the noise and power relationship. This area would research how close the minimum noise and minimum power points can get by modifying the blade geometry.

5 REFERENCES

[1] Electric VTOL News. “Jaunt Air Mobility Journey”. Retrieved on: https://evtol.news/jaunt-air-mobility/

[2] Moore, Jim. “Electric Air Taxis Aim For American Cities”. January 2021. Retrieved on: https://www.aopa.org/news-and-media/all-news/2021/january/21/electric-air-taxis-aim-for-american-cities

[3] Boyle, Alan. “Boeing’s Passenger Air Vehicle Prototype Rises Into the Sky for its first test flight”. January 2019. Retrieved on: https://www.geekwire.com/2019/boeings-passenger-air-vehicle-prototype-rises-air-first-test-flight/

[4] Electric VTOL News. “Joby Aviation S4”. Retrieved on: https://evtol.news/joby-s4

[5] Nolen, Billy. “The White House Summit on Advanced Air Mobility”. 3 August 2022. https://www.faa.gov/speeches/white-house-summit-advanced-air-mobility

[6] Read, Bill. “Sounding Out eVTOLs”. Royal Aeronautical Society. Published online 14 Sept. 2021. https://www.aerosociety.com/news/sounding-out-evtols/

[7] Wagner, Kate. “City Noise Might Be Making You Sick”. The Atlantic, published online 20 Feb. 2018. https://www.theatlantic.com/technology/archive/2018/02/city-noise-might-be-making-you-sick/553385/

[8] Angus, Leslie. “Broadband Noise Reduction on a Mini- UAV Propeller”. AIAA Aeroacoustics Conference. May 2008.

[9] Candeloro, Paolo, et al. “Small-scale rotor aeroacoustics for drone propulsion: a review of noise sources and control strategies”, University Cusano. Published online 8 October 2019.

[10] Peake, N. “The aeroacoustics of the Owl”. Lecture Notes in Mechanical Engineering, 2016. doi:10.1007/978-3-662-48868-3_2

[11] Jaworski, J.W.; Peake, N. “Aerodynamic noise from a poroelastic edge with implications for the silent flight of owls”. Journal of Fluid Mechanics 2013. doi:10.1017/jfm.2013.139.

[12] Avallone, F.; Van Der Velden, W.C.; Ragni, D.; Casalino, D. “Noise reduction mechanisms of sawtooth and combed-sawtooth trailing-edge serrations”. Journal of Fluid Mechanics 2018. doi:10.1017/jfm.2018.377

[13] Howe, M.S. “Noise produced by a sawtooth trailing edge”. The Journal of the Acoustical Society of America 1991, 90, 482–487. doi:10.1121/1.401273.

[14] Ning, Z.; Hu, H. “An Experimental Study on the Aerodynamic and Aeroacoustic Performances of a Bio-Inspired UAV Propeller”. 35th AIAA Applied Aerodynamics Conference, 2017. doi:10.2514/6.2017-3747.

[15] Bain, et al. “Aerodynamic and Acoustic Design of the Joby Aviation eVTOL Propeller”. Vertical Flight Society. 2021.

[16] Kobiki Noboru, et al. “A Study Of Closed Loop Control Of Active Tab With BVI Detection Method For Helicopter Noise Reduction”, Nihon University, Tokyo, Japan.

[17] Bebesel, Marius, et al. “Reduction of BVI Noise On Ground – In Flight Evaluation Of Closed-Loop Controller”, 28th EUROPEAN ROTORCRAFT FORUM, Bristol, UK, 2002

[18] Nguyen, Khan, et al. “Full-Scale Demonstration of Higher Harmonic Control for Noise and Vibration Reduction on the XV-15 Rotor”, NASA Ames Research Center, 2001

[19] Padthe, Ashwani, et al. “Comprehensive Numerical Assessment of Rotorcraft Vibration and Noise Control Using Microflaps”, Journal Of Aircraft, Vol. 53, 2016

[20] Beckman, Brian, and Gur Kimchi. “Active Airborne Noise Abatement”, Amazon Patent Application, 2018

[21] Gartenberg, Lenny. “Battery Centric Serial Hybrid Aircraft Performance and Design Space”. ERAU Thesis Dissertation. May 2017.

[22] Gartenberg, Lenny, Anderson, Richard P., and Martos, Borja. “Systems and methods for noise mitigation for hybrid and electric aircraft”. Embry Riddle Aeronautical University. Patent Number 10933977. March 2021.

[23] Santacruz, Xavier G. “Low-Tip-Speed High-Torque Proprotor Noise Approximation for Design Cycle Analysis”. ERAU Thesis Dissertation. May 2019.

[24] Leishman, Gordon J. “Principles of Helicopter Aerodynamics”. Cambridge Aerospace Series. 2006.

[25] Drela, M., & Youngren, H. Xfoil 6.94 user guide [Computer software manual]. The Massachusetts Institute of Technology. 2001.

[26] Gudmundsson, Snorry. “General Aviation Aircraft Design”. Butterworth-Heinemann. 2014.

[27] Sinibaldi, G. and Marino, L. “Experimental analysis on the noise of propellers for small UAV,” Applied Acoustics, Vol. 74, No. 1, 2013, pp. 79, 88.

[28] Salvati, D., and Drioli, C., “Acoustic Source Localization From Multirotor UAVs”, IEEE Transactions on Industrial Electronics, 2019.

[29] Intaratep, N., Alexander, N., Devenport, W., and Grace, S. M., “Experimental Study of Quadcopter Acoustics and Performance at Static Thrust Conditions,” 22nd AIAA/CEAS Aeroacoustics Conference, 2016.

[30] Hennes, C. C., Lopez, L. V., Shirey, J., Cheng, R., Erwin, J., Goldman, B. A., & Brentner, K. S. Psu-wopwop 3.4.3 user’s guide [Computer software manual]. The Pennsylvania State University. 2017.

[31] Lyrintzis, Anastasios S. “Surface Integral Methods in Computational Aeroacoustics-From the (CFD) near-field to the (Acoustic) Far-Field”. Presented at the CEAS Workshop “From CFD to CAA” in Athens, Greece. November 2002.

[32] Farassat, F. “Derivation of Formulations 1 and 1A of Farassat”. NASA Langley Research Center, Hampton, Virginia. March 2007.

[33] Brentner, Kenneth S. “Prediction of Helicopter Rotor Discrete Frequency Noise”. NASA Langley Research Center, Hampton, Virginia. 1986.

[34] Greenwood, Eric, Brentner, Kenneth, and Ted Gan, Ze Feng. “Challenges and Opportunities for Low Noise Electric Aircraft”. Article in International Journal of Aeroacoustics. June 2022.

[35] Farassat, F. “Theory of Noise Generation From Moving Bodies With an Application To Helicopter Rotors”. NASA Langley Research Center, Hampton, VA. 1975.

[36] McCormick, Barnes W. “Aerodynamics of V/STOL Flight”. The Pennsylvania State University. Academic Press. 1967.

[37] Castles, Walter Jr. and New, Noah C. “A Blade-Element Analysis for Lifting Rotors That is Applicable for Large Inflow and Blade Angles and any Reasonable Blade Geometry”. NACA. 1952.

[38] McCormick, Barnes W. “Aerodynamics, Aeronautics, and Flight Mechanics”. The Pennsylvania State University. John Wiley & Sons, Inc. 1995.

6 PUBLICATIONS

Roiati, R., Anderson, R., Collins, K., Hruswicki, P., Saini, V., Yang, X., and Sharma, N., “Development of a Multi-Rotor eVTOL Using RPM, Collective, and Cyclic Control”. Embry Riddle Aeronautical University. Presented to the Vertical Flight Society Technical Forum 78. May 2022.